mater.scichina.com link.springer.com https://doi.org/10.1007/s40843-026-4089-6

The properties and critical values of lunar glasses

Yue Huang[1,2†], Xiao Chen[2†], Lijian Song[2], Wei Xu[2], Meng Gao[2*], Juntao Huo[2,3*] and Jun-Qiang Wang[2,3*]

ABSTRACT Lunar glass is a unique amorphous material formed on the Moon through processes such as meteorite impacts and volcanic eruptions. It serves not only as a geological archive recording the history of lunar evolution, but also as a natural reservoir of matter generated under extreme conditions, including high vacuum, intense radiation, and large temperature fluctuations. This review systematically summarizes the current scientific understanding, resource potential, and materials science significance of lunar glass. Based on sample data from the Apollo and Chang'e-5 missions, we outline its classification and formation mechanisms, and elucidate its evolutionary pathways under different geological settings. We further summarize its multiscale structural characteristics and key physical properties, including thermal stability, mechanical behavior, and irradiation response, and evaluate the resource potential of H_2O and ^3He retained in lunar regolith glass and their roles in *in situ* resource utilization on the Moon. Finally, from a materials perspective, we discuss defect evolution and nanocrystallization of lunar glass over long timescales and under ion irradiation, and explore how these natural processes inspire the design of amorphous alloys and soft magnetic materials, thereby providing guidance for structure-property control of amorphous matter under extreme environments.

Keywords: lunar glass, space weathering, physical properties, *in situ* resource utilization, material design

INTRODUCTION

Glass stands as one of the most enduring and versatile materials, defined by its amorphous structure that lacks long-range atomic order and formed through the rapid cooling of melts that bypass crystallization. This unique structural feature endows glass with exceptional adaptability, encompassing a broad spectrum of compositions, microstructures, and functionalities. The earliest glassy materials emerged naturally long before deliberate human fabrication, with amber glass formed by solidifying lipids secreted by certain plants (Fig. 1a), oxide-based varieties like volcanic obsidian and meteorite-impact glass serving as nature's primordial experiments [1]. Even lightning strikes can forge natural glass, as intense heat melts silica-rich sand into thread-like fulgurite. As human civilizations mastered glassmaking technologies, from ancient Egyptian silica glass to medieval stained glass, oxide glasses evolved into foundational pillars of modern society (Fig. 1b, c). They enable pivotal applications such as architectural windows, optical lenses, microscopes, telescopes, and fiber optics [2,3]. The twentieth century marked a paradigm shift in glass science, expanding its horizons far beyond oxide systems. Polymeric glasses emerged alongside synthetic polymers, gaining indispensability due to their lightweight nature, mechanical flexibility, and ease of large-scale processing [4,5]. Small-molecule glasses (e.g., ritonavir) address low drug solubility, enhancing it by 2–3 orders of magnitude while boosting stability [4,6–8]. Chalcogenide glasses enable long-wave infrared optics, amorphous silicon powers thin-film electronics, and metallic/MOF glasses serve space gears and CO_2 separation [9–14]. These advances vividly underscore the inherent universality of the amorphous state, which transcends the bounds of distinct chemical bonding types, including covalent, molecular, metallic, coordinative, and mixed ionic-covalent bonding, across the diverse glass systems established beyond traditional oxide frameworks.

Against this backdrop of terrestrial glass evolution, lunar glass extends the concept of glass formation into an entirely distinct physical regime. Formed naturally through meteorite impacts, volcanic eruptions, and prolonged space weathering, lunar glass develops under extreme conditions, such as high vacuum, intense solar radiation, microgravity, and geological timescales spanning millions to billions of years [17–19]. These environments differ fundamentally from terrestrial glassmaking, producing amorphous materials with unique formation pathways: impact-derived lunar glass forms in milliseconds under extreme pressure, while volcanic glass cools slowly from lunar magma, and space-weathered glass accumulates atomic-scale damage from cosmic rays. Various lunar glasses are displayed in Fig. 1d–f, including the green glass samples with different sizes collected by Apollo 15 and black glass sample fragments in the Chang'e-5 (CE-5) lunar soil. Unlike laboratory-prepared glasses, lunar glass is a hyper-aged natural system that preserves direct records of lunar impact intensities, volcanic activity, and regolith evolution. The return of lunar samples by the Apollo missions and China's CE-5 mission has enabled unprecedented micro- and nanoscale investigations. CE-5 samples revealed glass beads with embedded nano-iron particles that record space weathering, while water trapped in lunar glass provides critical clues about the Moon's hydrological history [20–23]. This interdisciplinary bridge between planetary science and materials science not only unlocks lunar evolution secrets but also offers a model for extreme-condition material design, with significant implications

[1] School of Materials Science and Chemical Engineering, Ningbo University, Ningbo 315211, China
[2] Ningbo Institute of Materials Technology and Engineering, Chinese Academy of Sciences, Ningbo 315201, China
[3] Center of Materials Science and Optoelectronics Engineering, University of Chinese Academy of Sciences, Beijing 100049, China
† Equally contributed to this work.
* Corresponding author (email: gaomeng@nimte.ac.cn; huojuntao@nimte.ac.cn; jqwang@nimte.ac.cn)

© Science China Press 2026

Figure 1 Representative natural, artificial, and lunar glasses. (a) Natural amber, a fossilized plant resin representing a naturally occurring amorphous material. (b, c) Artificial oxide glasses, including optical lenses and decorative glassware. (d) Diverse lunar glass particles (⩾200 μm size fraction) from Apollo 15 soils. Reprinted with permission from Ref. [15]. Copyright 2019, John Wiley and Sons. (e) Green volcanic glass beads collected during the Apollo 15 mission. (f) Black glass fragments in Chang'e-5 (CE-5) lunar soil, with a scale bar of 0.5 mm. Reprinted with permission from Ref. [16]. Copyright 2021, National Science Review.

for *in situ* resource utilization (ISRU). For example, lunar glass could be melted to produce oxygen or structural ceramics critical for the construction of lunar bases.

Motivated by these advances, this review presents a comprehensive overview of lunar glass from a materials science perspective. We first summarize its classification (impact-derived, volcanic, and space-weathered varieties) and diverse formation mechanisms, integrating insights from CE-5 and Apollo sample analyses. We then examine its structural characteristics from nanoscale inclusions to atomic bonding and key physical properties, including thermal stability, mechanical behavior, and long-term aging effects, comparing them with terrestrial counterparts. Finally, we highlight the broader implications of lunar glass: its role in deciphering planetary evolution, its potential for ISRU in lunar base construction, and its value as a model system for understanding amorphous matter under extreme conditions. By synthesizing these dimensions, this review aims to provide a cohesive framework for future research at the intersection of planetary science and advanced materials engineering, bridging celestial exploration with technological innovation.

OVERVIEW OF LUNAR GLASS

Lunar glass stands as a crucial and ubiquitous component in the surficial lunar regolith. It is by no means an artificial product, but rather a direct outcome and faithful record of the Moon's extreme natural environment, forged by non-equilibrium processes like volcanic eruptions, hypervelocity meteorite impacts, and prolonged solar wind irradiation [22,24]. Derived from high-temperature molten materials formed during these intense events, lunar glass stands in stark contrast to crystalline lithic clasts [25]. Unlike minerals with long-range ordered atomic lattices (Fig. 2a–c), lunar glass exhibits distinct amorphous features, lacking grain boundaries and composition segregation. What is more, there appears the pronounced internal homogeneity within the lunar glass sample, with its chemical components uniformly distributed across the disordered atomic network, as shown in Fig. 2d–f. This structural uniqueness endows it with exceptional stability, allowing it to preserve pristine information about lunar processes over billions of years.

Research into lunar glass traced its origins to the Apollo missions in the 20th century [27–29]. During these landmark missions, astronauts brought back lunar samples from equatorial regions, enabling scientists to systematically identify abundant impact-melted glass spherules, irregular fragments, and volcanic glass formed by ancient fire-fountain eruptions. Early studies employed optical microscopy, X-ray diffraction, and elemental analysis to characterize these glasses [15,30–33]. The preliminary researches mainly focused on correlations between their morphological features (e.g., spherical shapes from rapid cooling, irregular edges from impact fragmentation), chemical compo-

© Science China Press 2026

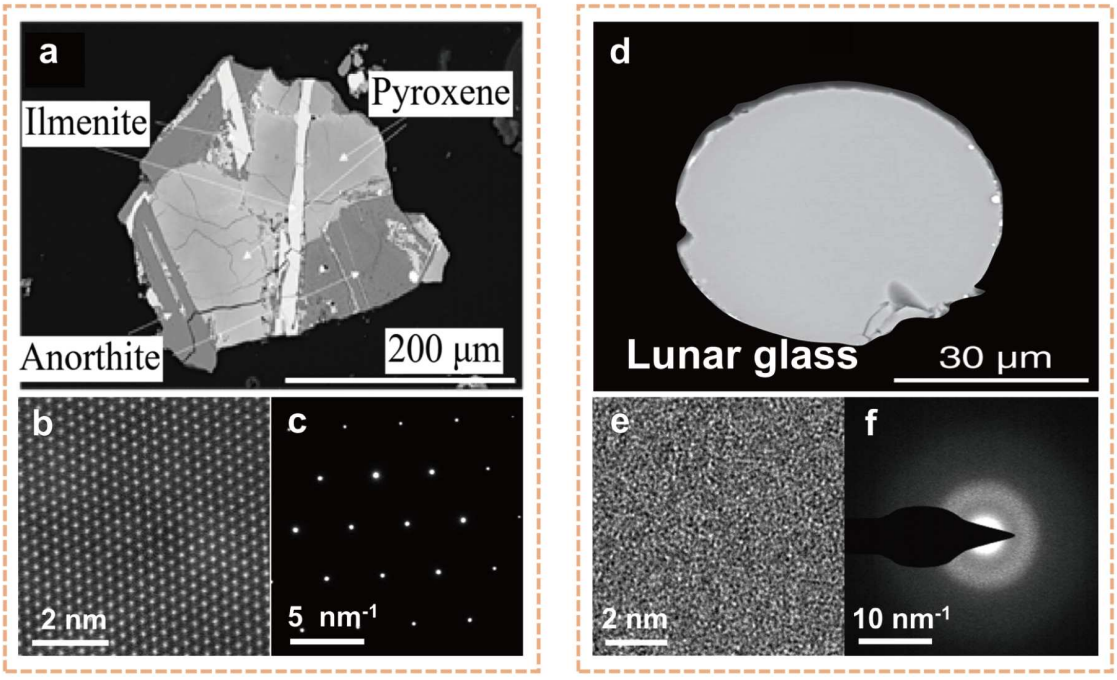

Figure 2 Microstructural and crystallographic characterization of lunar minerals and impact glass. (a) Rock fragment containing anorthite ($CaAl_2Si_2O_8$), pyroxene ($(Ca,Fe,Mg)_2Si_2O_6$), and ilmenite ($FeTiO_3$). Reprinted with permission from Ref. [25]. Copyright 2024, Springer Nature. (b, c) High-resolution transmission electron microscopy (HRTEM) image and corresponding electron diffraction pattern of crystalline ilmenite. (d) Impact glass fragment containing relic mineral inclusions. Reprinted with permission from Ref. [26]. Copyright 2024, The American Association for the Advancement of Science. (e, f) HRTEM image and electron diffraction pattern of lunar soil glass, revealing its amorphous structure.

sitions (e.g., high-titanium vs. ultralow-titanium volcanic glass), and space weathering effects (e.g., surface nanophase iron formation). These findings laid a solid experimental foundation for subsequent lunar glass research, confirming that the Moon's surface has long been shaped by intense impact and volcanic activities.

Entering the 21st century, lunar glass research achieved breakthrough progress, particularly with the successful sample return from the young basaltic region in the northern Oceanus Procellarum by the CE-5 mission [16,34,35]. Unlike previous Apollo samples collected near the equator, CE-5's sampling site (51.916°W, 43.058°N) is the highest-latitude lunar soil returned to date, offering a unique window into a previously unexplored lunar environment. Studies revealed that CE-5 samples not only contained classic spherical impact glass beads but also uniquely shaped natural glass fibers, which had never been reported in prior lunar samples [36]. This discovery indicated a relatively mild impact environment at the landing site, with shock pressures ranging from 17 to 25.8 GPa. More significantly, the detection of substantial water (with a surface-high, interior-low concentration gradient) derived from solar wind injection within impact glass beads confirmed lunar glass as a vital "H_2O reservoir" on the Moon. Additionally, its disordered structure demonstrates exceptional storage capacity for strategic resources like helium-3 (^3He), which is trapped in glass layers on ilmenite particles as nanoscale bubbles, greatly expanding the cognitive boundaries for ISRU of lunar resources [31,37–39].

Lunar glass serves as a pivotal material linking the Moon's past and future [40]. It acts as a "chronicle" that deciphers billions of years of lunar evolution, preserving information about volcanic activity, impact dynamics, space weathering, and water origins. It also functions as a "warehouse" storing critical resources estimated to hold 270 billion tons of H_2O and 260,000 tons of ^3He, which are essential for human permanent settlement on the Moon [15,30–33]. Furthermore, it stands as an "inspiration source" for designing future advanced materials, as its long-term aging and space weathering-induced microstructural evolution provide valuable insights for developing terrestrial ultra-stable glasses and high-performance soft magnetic materials [41]. In-depth research on lunar glass thus constitutes the pivotal bridge connecting lunar science from exploration to utilization, laying the groundwork for both fundamental planetary research and practical deep space exploration engineering.

CLASSIFICATION AND FORMATION OF LUNAR GLASS

Based on distinct formation mechanisms shaped by the Moon's extreme non-equilibrium processes, lunar glass is systematically classified into four primary categories. Volcanic glasses originate from deep magmatic eruptions, while impact glasses form via high-velocity meteorite bombardment. Irradiation glasses arise from prolonged solar wind ion irradiation of regolith grains, and vapor deposition glasses result from the rapid condensation of impact-induced silicate vapors. Each type exhibits unique physicochemical properties that faithfully reflect its specific geological history, serving as "geological archives" for decoding lunar evolution.

Volcanic glass

Volcanic glass is a direct product of lunar internal magmatic activity, primarily originating from early lunar volcanic eruptions (Fig. 3a) [42,43]. During intense "fire fountain" eruptions,

© Science China Press 2026

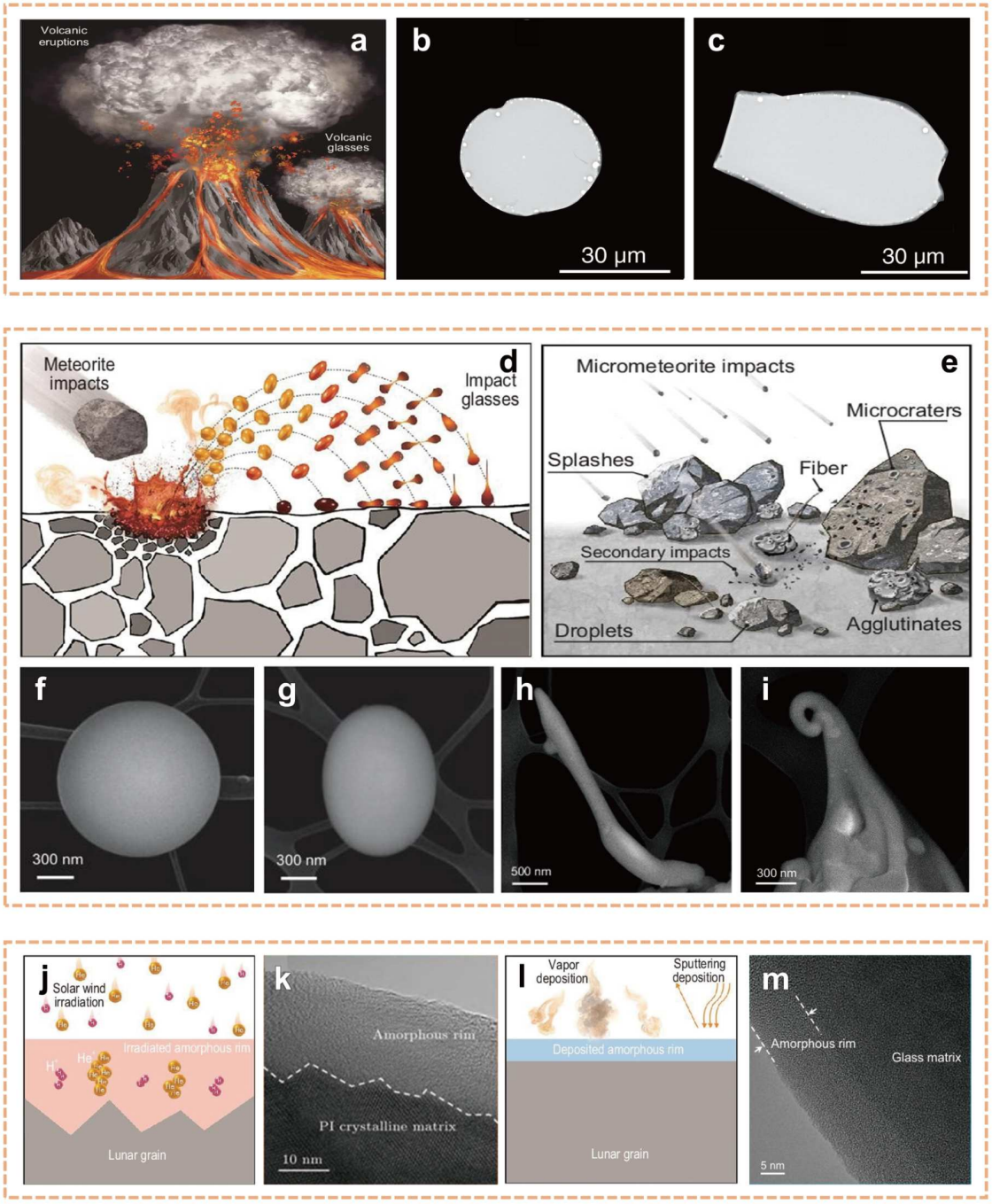

Figure 3 Formation and modification mechanisms of lunar glasses. (a) Schematic illustration of volcanic eruptions ejecting molten droplets that rapidly quench to form volcanic glass particles in pyroclastic deposits. Reprinted with permission from Ref. [45]. Copyright 2023, Oxford University Press. (b, c) Optical images of representative volcanic glass beads. Reprinted with permission from Ref. [26]. Copyright 2024, The American Association for the Advancement of Science. (d, e) Schematic illustration of frequent micrometeorite impacts inducing localized melting and rapid quenching, producing agglutinate-like, splash-like, droplet-like, ring-like glasses associated with microcraters, as well as glass fibers; (f, g) Impact glass beads with diverse morphologies in CE-5 lunar soils; (h, i) Unique glass fibers observed in CE-5 lunar soils; (j) Schematic illustration of solar wind irradiation damaging surface structures of lunar grains; (k) Irradiation-induced non-uniform amorphous rims on lunar grains; (l) Schematic illustration of impact-generated vapor deposition on lunar grain surface; (m) Uniform vapor-deposited amorphous rims observed on CE-5 soil particles. Reprinted with permission from Ref. [45]. Copyright 2023, Oxford University Press.

low-viscosity basaltic magma is ejected into the Moon's vacuum environment, where the absence of atmospheric heat transfer causes molten droplets to rapidly cool and quench during flight. This ultrafast cooling with rates exceeding 10^4 K/s freezes the atomic structure in a disordered state, forming spherical or ellipsoidal glass beads (Fig. 3b, c) that preserve the chemical signature of the lunar interior [26].

Unlike impact-derived glasses, volcanic glasses typically

© Science China Press 2026

exhibit highly homogeneous chemical compositions, rarely containing vesicles or unmelted mineral inclusions, and lack the Fe-Ni metal particles commonly introduced by meteoritic contamination in impact glasses [44]. Geochemically, they are basaltic to picritic silicate glasses with SiO_2 contents ranging from ~40 wt% to 50 wt%. Based on TiO_2 concentration, volcanic glasses are classified into two distinct groups: ultralow-titanium (TiO_2 < 0.5 wt%, MgO/Al_2O_3 > 1.25 wt%) and high-titanium ($TiO_2 \approx 6$ wt%), both with FeO content around 19 wt%–22 wt% [27]. The high-titanium type exhibits superior structural stability due to Fe^{2+}-Ti^{4+} charge transfer effects, which strengthen the atomic network and inhibit thermal relaxation over geological timescales.

Microstructurally, volcanic glass features a highly uniform distribution of chemical components and a dense amorphous network structure. It is typically free of impact-induced nanophase iron particles ($npFe^0$) and exogenous mineral inclusions, resulting in higher thermal stability compared to defect-rich impact glasses [39,46]. Notably, in the CE-5 lunar regolith, volcanic glass is extremely rare and its abundance is far lower than that of impact glass. This scarcity not only confirms that the scale of late-stage lunar volcanism had significantly diminished by 2.0 billion years ago (the age of CE-5 basalts) but also highlights these rare, young volcanic glasses as critical samples for investigating the final stages of the Moon's thermal evolution [44,47]. Their chemical composition and structural state can reveal the cooling history of the lunar mantle and the degree of magmatic differentiation during the late lunar period.

Impact glass

Impact glass represents the most abundant glass type on the lunar surface, accounting for 11.6%–20.0% of CE-5 regolith and even higher proportions (25.4%–72.3%) in Apollo samples [27,48,45]. It is generated by the hypervelocity impacts of meteorites or micrometeorites (typically traveling at 15–25 km/s) on the lunar regolith, which instantaneously generate extreme pressures (>100 GPa) and temperatures (>1500 °C) that melt local rocks and minerals. The molten material is then ejected, rotated, and rapidly quenched as it spreads across the lunar surface (Fig. 3d, e) [19,40,47,49–52]. Due to the stochastic nature and complexity of impact processes, including variations in impactor size, velocity, and target rock composition, impact glasses exhibit significant diversity in morphology and composition. They appear as regular spheres (Fig. 3f), ellipsoids (Fig. 3g), dumbbells, teardrops, and other rotational shapes, with sizes ranging from nanometers to centimeters.

The chemical composition of impact glass is highly complex and heterogeneous, primarily inheriting the geochemical signatures of the target rocks. The provenance of these glasses can be effectively distinguished based on the CaO/Al_2O_3 ratio: glasses of highland origin (dominated by plagioclase) typically have a ratio of less than 0.75, whereas those of mare origin (rich in pyroxene and ilmenite) generally exceed 0.7 [27]. In contrast to pure volcanic glasses, impact glasses often entrap exogenous meteoritic materials. Zeigler *et al.* identified metal particles with characteristic meteoritic Fe-Ni ratios (Fe:Ni ≈ 94:6) in Apollo 16 samples, confirming the material contribution from the impactor [27]. Microstructurally, $npFe^0$ particles ranging from 5 to 50 nm are distributed within the interior and on the surface, derived from the disproportionation reaction of Fe^{2+} under high pressure and temperature during impact [53]. These $npFe^0$ particles significantly alter the optical properties of impact glass, causing the "darkening and reddening" effects associated with space weathering.

Notably, researchers have discovered unique ultra-long glass fibers in the CE-5 lunar regolith samples (Fig. 3h, i), a feature never reported in previous Apollo or Luna missions. These glass fibers have diameters as fine as tens of nanometers (one-thousandth the diameter of a human hair) and elongation exceeding 50, far surpassing the elongation of Apollo regolith particles (typically 1–3) [48,45]. This distinctive morphology corresponds to a gentle impact environment characterized by shock pressures of 17–25.8 GPa [54]. Unlike high-velocity impacts that produce low-viscosity melts forming spherical beads, moderate-velocity impacts generate high-viscosity melts that undergo continuous thermoplastic flow. This allows impact forces to pull the melt into ultra-long fibers analogous to dripping syrup forming thin threads.

Irradiation amorphous rims

Irradiation amorphous rims are formed when lunar surface particles undergo prolonged irradiation by high-energy solar wind ions (H^+, He^{2+}), resulting in the destruction of surface crystal structures and the formation of irradiation-induced amorphous edges (Fig. 3j). It is a direct and ubiquitous product of space weathering, with its formation mechanism closely linked to the Moon's lack of a protective magnetic field and atmosphere [55]. The formation process involves the long-term implantation of solar wind ions (energy 0.3–3 keV) into particle surfaces. These high-energy ions collide with lattice atoms, displacing them from their equilibrium positions and generating numerous defects, including vacancies, interstitials, and dislocations. Over millions of years, this cumulative radiation damage disrupts the long-range order of the crystal lattice, transforming the surface layer into an amorphous state.

Microstructurally, irradiation amorphous rims appear to envelop the surface of the host particle, with a thickness typically ranging from tens to hundreds of nanometers. This thickness is primarily determined by the penetration depth of solar wind ions and the mineralogy of the particle (e.g., plagioclase is more susceptible to amorphization than ilmenite [56]). In contrast to the smooth interfaces observed in vapor-deposited amorphous rims, Transmission Electron Microscopy (TEM) reveals a distinct jagged interface between the irradiation glass and the underlying crystalline substrate (Fig. 3k). It is a characteristic feature indicative of anisotropic radiation damage, as ions preferentially penetrate along crystal defects and low-density planes. Chemically, the irradiation amorphous rims largely inherit the composition of the host mineral, exhibiting no significant elemental enrichment or depletion, which distinguishes it from compositionally modified vapor deposition amorphous rims.

Li *et al.* [57] demonstrated that the thickness of irradiation rims on CE-5 particles exhibits a positive correlation with surface exposure time (within the saturation threshold). Using this relationship, the calculated average surface exposure age of the CE-5 lunar regolith is approximately 2 million years [45,55,58]. Furthermore, the isotope ratios of H and He trapped within these rims are highly consistent with those of the modern solar wind, confirming that they are the direct products of solar wind implantation [13,16]. These trapped ions not only validate the formation mechanism of irradiation glass but also provide

© Science China Press 2026

insights into the long-term evolution of the solar wind.

Vapor deposition amorphous rims

Vapor-deposited amorphous rims are a product of non-equilibrium processes on the lunar surface triggered by high-energy impact events. It is essentially formed through the rapid condensation (vapor deposition) of high-temperature silicate vapors onto the surfaces of lunar regolith grains. Unlike impact melt glasses, which undergo a liquid-to-solid transition, vapor-deposited amorphous rims bypass the melt phase, transforming directly from the gaseous state into an amorphous solid film [36,48,45]. This direct gas-to-amorphous-solid transformation gives it distinct structural and compositional features.

The formation mechanism originates from high-velocity impacts by meteorites or micrometeorites, which instantaneously vaporize target silicate rocks into Si-O-rich high-temperature vapors at temperatures exceeding 3000 °C (Fig. 3l). As these vapors diffuse onto the surfaces of surrounding cooler particles (at lunar surface temperatures of ~200 K), the extremely high cooling rate (~10^6 K/s) kinetically inhibits atomic ordering, resulting in deposition as a dense amorphous film [56]. Morphologically and microstructurally, this type of glass manifests as continuous and dense nanoscale thin films covering host grains rather than as independent particles [56]. This deposited film exhibits a smooth interfacial transition with the substrate due to the conformal nature of vapor condensation (Fig. 3m). Its internal structure consists of densely arranged Si-O tetrahedra, free of pores or inclusions, demonstrating exceptionally high structural homogeneity.

Chemical analysis indicates that vapor-deposited amorphous rims are primarily composed of a SiO_2-rich amorphous phase, significantly depleted in refractory elements such as Mg and Al, and devoid of $npFe^0$. This composition distinguishes it markedly from impact melt glasses, which are typically rich in iron and impurities inherited from target rocks. Comparative planetary studies reveal striking differences between CE-5 and Apollo samples: the average thickness of vapor-deposited rims in CE-5 is approximately 7 nm (range: 2.8–16.3 nm), significantly thinner than those in Apollo samples (50–60 nm) [45]. This discrepancy reflects a relatively mild impact environment at the CE-5 landing site, where lower-velocity impacts generate less silicate vapor and result in thinner deposition layers. For instance, the deposition layer on Apollo 11 high-titanium glass surfaces possesses a SiO_2 content exceeding 90 wt%, far higher than that of its plagioclase host ($SiO_2 \approx 60$ wt%). Such a pronounced compositional discrepancy strongly confirms a vapor-condensation origin rather than *in situ* melting.

PHYSICAL PROPERTIES OF LUNAR GLASS

Optical properties

The optical properties of lunar regolith glass stand as a foundational pillar for identifying the composition of lunar materials, inferring their formation mechanisms, and evaluating the extent of space weathering [19,59–61]. Unlike crystalline minerals such as olivine and pyroxene, which exhibit distinct and sharp absorption peaks rooted in their ordered atomic structures, lunar glass typically presents broad and shallow absorption features. This unique spectral trait stems from its amorphous nature, where the lack of long-range atomic ordering blurs the electronic transition pathways of metal ions. The spectral behavior of lunar glass is dually governed by its chemical composition with Fe and Ti contents playing dominant roles, and its microstructure, including the distribution of nanoscale inclusions and structural defects [36]. These combined factors make lunar glass spectra a rich source of information about the lunar surface's evolutionary history.

The visible-near infrared (VNIR) spectra of lunar glass are primarily regulated by transition metal ions within the glass network. As demonstrated in studies by Cannon *et al.* [62] and Hu *et al.* [21], lunar glass consistently exhibits broad absorption bands near 1000 and 2000 nm, which are mainly induced by the crystal field transitions of Fe^{2+} ions in octahedral and tetrahedral coordination environments, respectively [20]. However, variations in the chemical composition of the glass result in significant spectral changes (Fig. 4a) [62]. Low-iron/highland glass ("Moon_Crust") displays the highest albedo and relatively flat spectral features due to the scarcity of iron, which minimizes Fe-related absorptions. This type of glass generally presents a light or blue-green hue, a visual characteristic that aligns with its spectral neutrality. In contrast, Fe-rich/Ti-rich glasses (such as "Moon Mare/Orange/Red" variants) exhibit strong ultraviolet-visible (UV-VIS) absorption as TiO_2 content increases. Specifically, high-titanium glass (e.g., Apollo 17 orange glass) generates a strong absorption edge at shorter wavelengths due to the Fe^{2+}-Ti^{4+} charge transfer effect [62]. This effect suppresses reflectance in the blue-visible range while enhancing it in the near-infrared, leading to spectral "reddening" and an orange-red appearance (evident in the red and orange lines in Fig. 4a). Low-titanium, high-magnesium green glass, on the other hand, features a characteristic reflectance peak near 550 nm, a result of reduced Fe^{2+}-Ti^{4+} charge transfer and specific crystal field transitions of Fe^{2+}, giving it a distinct green coloration.

The experimental spectra of these synthetic glasses have been successfully applied to the interpretation of orbital remote sensing data. By leveraging Moon Mineralogy Mapper (M^3) data combined with spectral unmixing models (Fig. 4b), researchers effectively isolated the spectral signals of glass from mixed lunar surface materials [62]. This approach enabled the successful identification of glass-rich pyroclastic deposits at Alphonsus crater, where the modeled glass spectral fractions were concentrated around volcanic vents and gradually diminished outward. This achievement not only validated the effectiveness of laboratory spectral models in planetary remote sensing but also provided critical insights into the distribution of volcanic activity on the Moon.

Beyond intrinsic chemical composition, nanophase reduced iron ($npFe^0$) particles formed during space weathering are the core intrinsic factor regulating the optical properties of lunar glass [19,38,55,63,64]. According to Hapke's classic theory [51] and recent analysis of CE-5 samples by Zhao *et al.* [48], the size of $npFe^0$ particles exerts distinct impacts on the spectra. These particles are concentrated in the 5–50 nm range (Fig. 4c, d), and their abundance and size directly control the spectral "darkening" and "reddening" effects. When the $npFe^0$ diameter is <20 nm, the particles strongly scatter and absorb short-wavelength light while enhancing reflectance within the near-infrared band (1000–2500 nm), resulting in the "reddening" phenomenon. Conversely, particles with diameters >40 nm significantly reduce reflectance across the entire spectral range with visible region reflectance dropping from 80% to below 40%, producing a pronounced "darkening" effect [51,52,65,66]. Pieters *et al.*

© Science China Press 2026

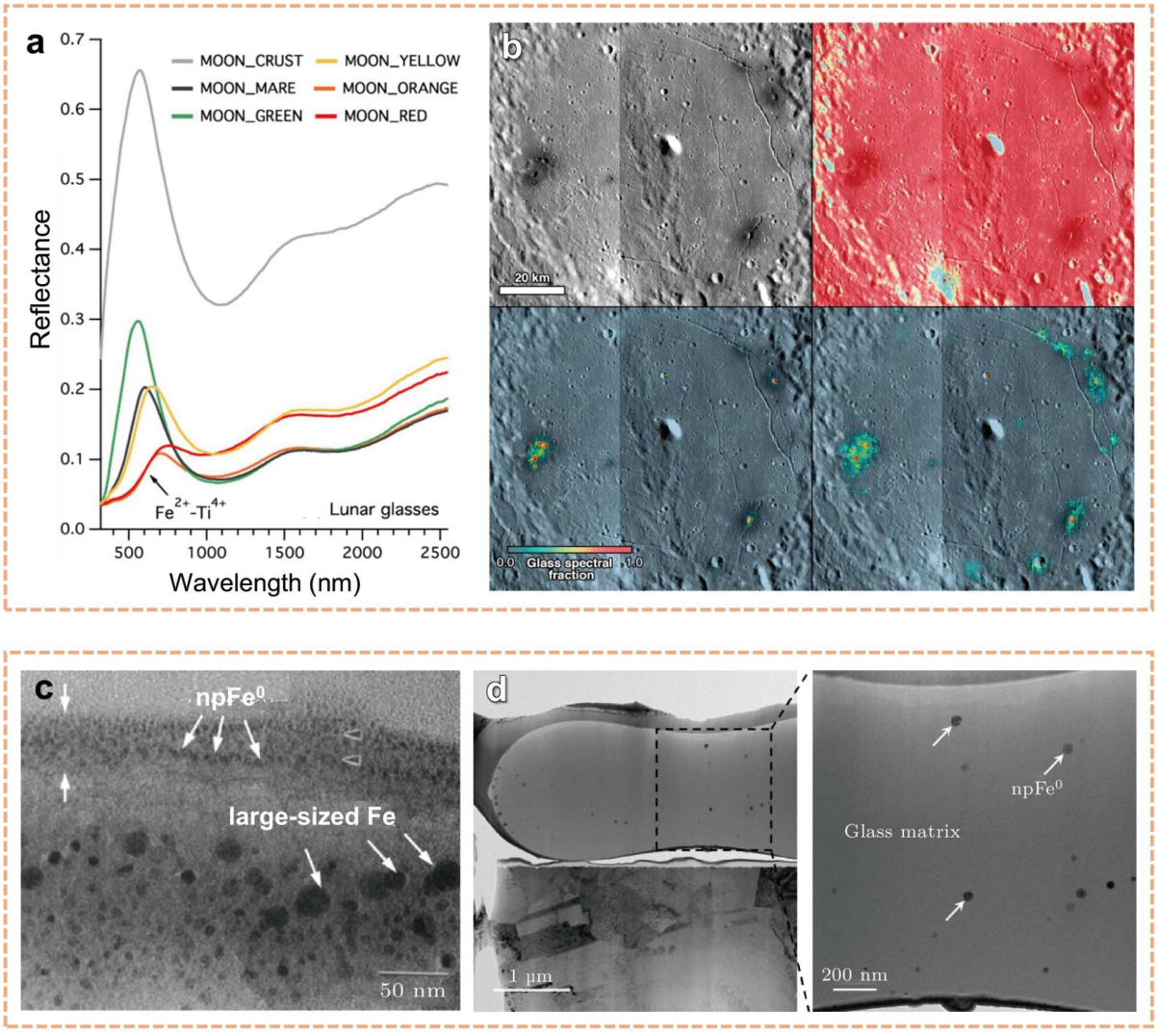

Figure 4 Spectral characteristics and nanophase iron in lunar glasses. (a) Visible-near-infrared (VNIR) reflectance spectra of compositionally distinct synthetic lunar glasses; (b) Validation of the glass spectral unmixing model using Moon Mineralogy Mapper (M^3) scenes over the Alphonsus crater. Reprinted with permission from Ref. [62]. Copyright 2017, John Wiley and Sons. (c) TEM image showing small- and large-sized nanophase iron (np-Fe^0) particles within agglutinates from Apollo lunar soils; (d) TEM image of an impact glass bead from CE-5 lunar soil, revealing np-Fe^0 particles embedded in the glass matrix. Reprinted with permission from Ref. [49]. Copyright 2010, John Wiley and Sons.

further confirmed through fine particle separation experiments that fine fractions (<45 μm) containing concentrated $npFe^0$ dominate the contributions to spectral reddening and darkening during space weathering [38]. This mechanism has been fully verified in Apollo regolith glasses, where the cumulative effect of space weathering over billions of years led to high $npFe^0$ contents. Notably, the $npFe^0$ content in Apollo regolith glass (0.1%-0.5 wt%) is significantly higher than that in CE-5 samples (0.03%-0.1 wt%), a difference attributed to the younger geological age of the CE-5 sampling region. This discrepancy is the key reason for the more pronounced spectral reddening observed in Apollo samples, highlighting the role of $npFe^0$ as a "chronometer" for space weathering intensity.

Thermal stability

Lunar glass, as a natural amorphous material, endures the lunar surface's extreme diurnal temperature swings (a 310 K variation) and prolonged geological weathering. It boasts thermal stability that directly dictates three core aspects: its structural intactness (critical for preserving ancient lunar records), the efficiency of storing embedded resources, and its feasibility for ISRU in future lunar missions.

Based on studies of single lunar glass particle from CE-5 regolith [16,36,67–70], impact-formed glassy particles (20–100 μm in diameter) mostly take spherical or ellipsoidal shapes (Fig. 5a), which locks the material into a metastable amorphous state before crystallization can initiate. These particles exhibit notably higher intrinsic thermal stability than terrestrial glassy materials (Fig. 5b). To mimic their natural formation conditions, researchers used Flash DSC at a 10 K/s heating rate (closely matching the rapid cooling rate of impact melts) to quantify their thermal behavior [71]. Clearly, the detailed thermodynamic parameters are: the glass transition temperature (T_g) ranges 944–968 K, crystallization temperature (T_x) hits 1251–1260 K, and the supercooled liquid phase width ($T_x - T_g$) spans 283–316 K. Such elevated T_g and broad super-

© Science China Press 2026

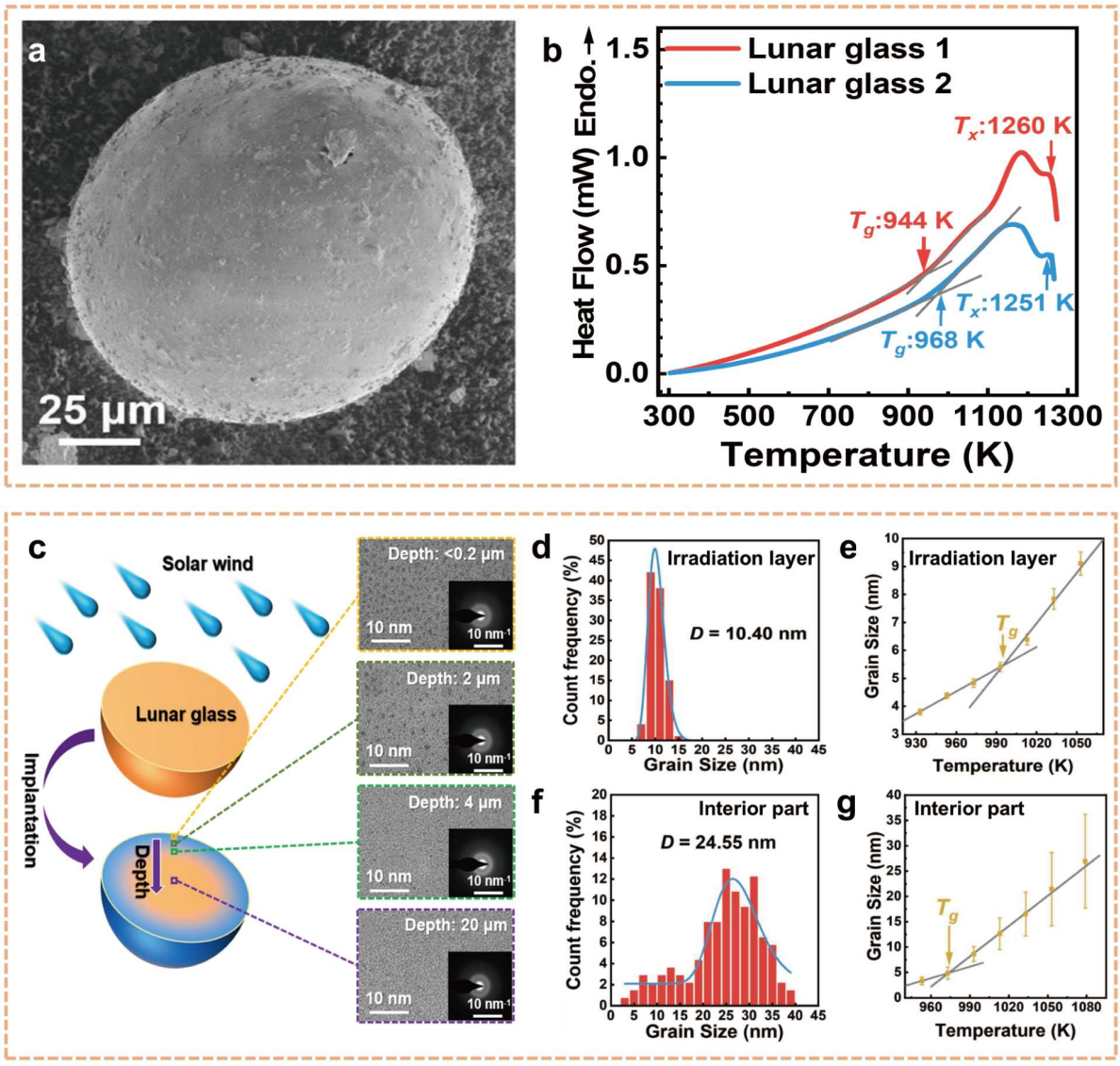

Figure 5 Solar-wind-induced structural modification and thermal behavior of lunar glass spheres from CE-5 soils. (a) Scanning electron microscopy (SEM) image of a representative lunar glass sphere (~25 μm in diameter); (b) Flash differential scanning calorimetry (Flash DSC) curves of two lunar glass samples, showing T_g and T_x; (c) Schematic illustration of solar wind implantation on lunar glass surfaces, forming an irradiation-modified surface layer; insets show HRTEM images acquired at different depths from the surface; (d, f) Grain size distributions of nanocrystalline domains in the irradiation layer and the interior region of lunar glass after *in situ* TEM heating; (e, g) Temperature-dependent grain growth behavior in the irradiation layer and the interior region, respectively; the intersection of two grain-growth regimes corresponds to the apparent T_g. Reprinted with permission from Ref. [71]. Copyright 2025, Springer Nature.

cooled region mean lunar glass resists both thermal relaxation (which softens amorphous materials) and crystallization, forming the physical foundation for its persistence across billions of years of lunar geological history.

As noted, the solar wind dominated by H ions strongly interacts with lunar regolith, altering lunar glass structures. Fig. 5c shows long-term solar wind irradiation forms a thin surface irradiation layer, H^+ ions implant into the glass network, causing local structural relaxation, but the glass's high T_g prevents this from triggering crystallization, so the overall structure remains amorphous. HRTEM images reveal 2–3 nm dark clusters (likely nascent Fe-rich nanophases) evenly distributed in this surface layer. The selected area electron diffraction (SAED) patterns (insets of Fig. 5c) confirm the persistent amorphous matrix. As depth increases, these clusters fade: at ~4 μm deep, they nearly disappear, signaling that solar wind's implantation effect weakens sharply. In the particle's central region (~20 μm deep), no clusters exist, confining the irradiation-altered layer to depths <4 μm. Statistical measurements of nanocrystal sizes (Fig. 5d, e) after *in situ* heating show the irradiation layer's nanocrystals have an average 10.40 nm grain size, uniformly dispersed in the amorphous matrix. Temperature dictates their growth, below ~994 K (the T_g), atomic diffusivity is low, so crystals grow slowly via individual grain expansion. Above T_g, the supercooled liquid's enhanced diffusivity accelerates growth. In the particle's interior (Fig. 5f, g), nanocrystals average 24.55 nm (5–40 nm range), a broad distribution reflecting the random nucleation and growth of Fe nanocrystals during the

© Science China Press 2026

glass's formation.

Crucially, these structural traits tie tightly to lunar glass's thermal stability. The extreme lunar diurnal temperatures never approach the glass's high T_g, so surface nanocrystals cannot grow rapidly or trigger bulk crystallization, and the shallow irradiation layer leaves the glass's core structure thermally resilient. This balance means the material retains its integrity despite space weathering. This combination of bulk thermal stability and surface modifiability carries practical promise. For *in situ* lunar missions, the surface nanocrystals could act as catalytic sites for resource extraction, while the durable glass bulk serves as a stable carrier material. It also lets researchers use glass's nanocrystal growth (regulated by T_g) to infer space weathering durations, aiding lunar surface dating.

Mechanical properties

Beyond thermal stability, the most striking feature of lunar glass lies in its "hyper-aging", a unique physical aging process shaped by billions of years of lunar geological evolution. Unlike laboratory-simulated aging, this natural process is driven by the moon's extreme intrinsic conditions: drastic diurnal temperature cycles, persistent solar wind irradiation, and ultra-high vacuum, making it impossible to fully replicate on Earth [72,73]. This hyper-aging effect is not accidental but rooted in the material's inherent nature: as non-equilibrium amorphous materials, glasses inherently tend to relax toward lower energy states over time [74,75]. What amplifies this relaxation in lunar glass is its dual background: on one hand, it forms via rapid quenching of impact melts, which locks it into a high-energy metastable state; on the other hand, the long-term lunar environmental stimuli continuously drive structural adjustment. To better understand how hyper-aging modifies mechanical properties, two core mechanical properties can be investigated. Elastic modulus reflects a material's resistance to elastic deformation, determined solely by its intrinsic atomic structure and interatomic bonding strength. By contrast, hardness describes the ability to withstand surface indentation, as it relies not only on the original structure but also on the dynamic plastic deformation mechanisms activated during loading.

To quantify the mechanical effects of hyper-aging, Chen *et al.* [76] conducted comparative micromechanical analyses of CE-5 lunar glasses: natural hyper-aged samples (H-A) and their chemically identical counterparts rejuvenated via laboratory remelting and quenching (L-R, Liquid-quenched Rejuvenated)

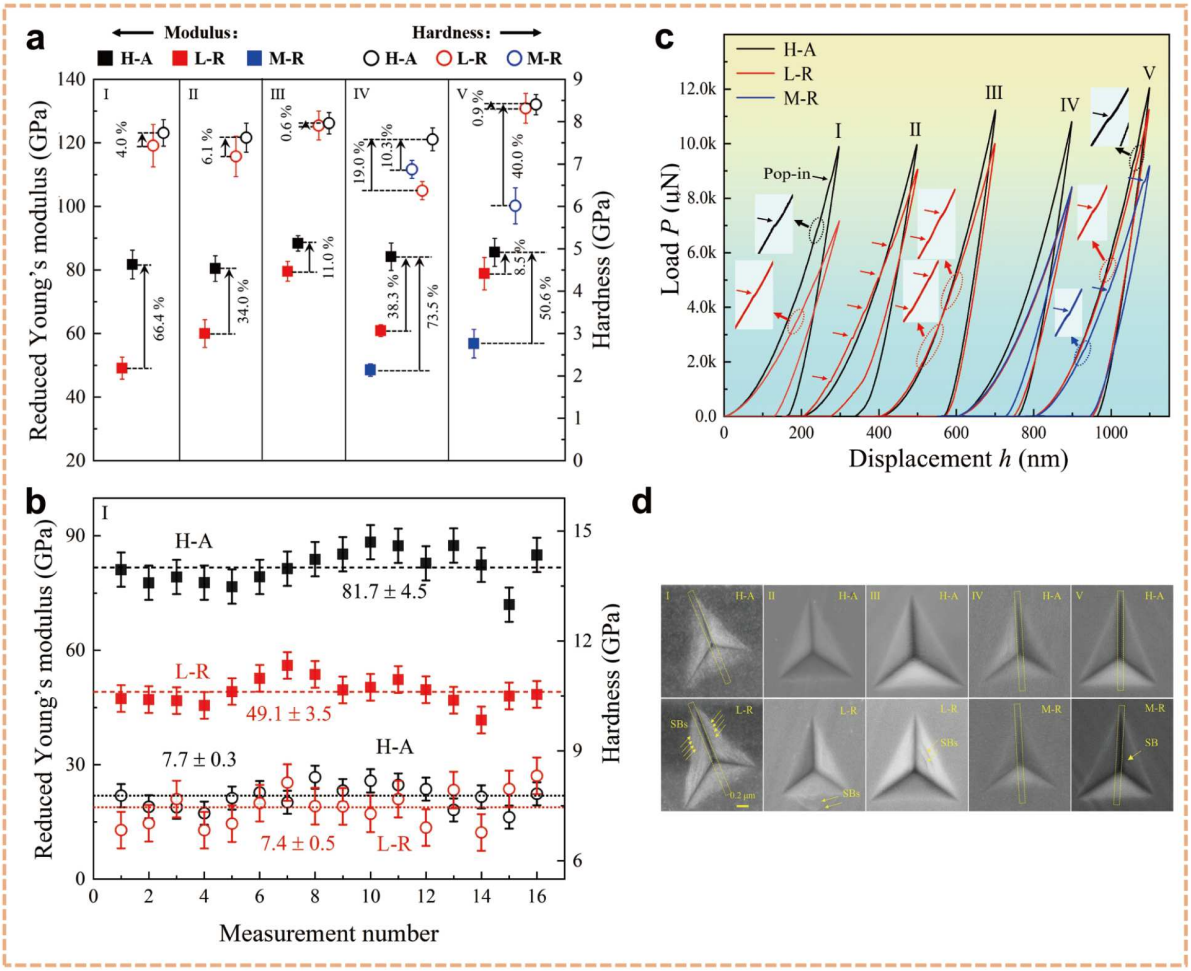

Figure 6 Mechanical properties of lunar glass particles before and after rejuvenation. (a, b) Comparison of reduced Young's modulus and hardness between the as-prepared (H-A) and rejuvenated (L-R and M-R) lunar glass particles measured at multiple locations (I–V); error bars represent standard deviations; (c) Representative load-displacement (*P-h*) curves obtained from nanoindentation tests, illustrating the softening behavior after rejuvenation; (d) Residual indent morphologies of H-A and rejuvenated lunar glass particles (I–V), revealing differences in deformation features after mechanical rejuvenation. Reprinted with permission from Ref. [76]. Copyright 2023, American Association for the Advancement of Science.

© Science China Press 2026

(Fig. 6a, b). The H-A samples exhibited a remarkable 73.5% increase in Young's modulus compared to L-R samples, an unprecedented enhancement for glassy materials, underscoring the profound impact of long-term aging. Notably, hardness variation was far less dramatic, revealing a unique decoupling between modulus and hardness during hyper-aging, a phenomenon rarely observed in terrestrial glasses. The above results show the obvious decoupling behaviors between elastic modulus and hardness in the lunar glassy particles.

To uncover this decoupling mechanism, researchers analyzed load-displacement (P-h) curves and residual indent morphologies (Fig. 6c, d). For four of the five glassy particles (I, II, III, V), the P-h curves showed "pop-ins" (marked by arrows), which are the signatures of shear band (SB) activation and a key plastic deformation mechanism in glasses. Rejuvenated L-R samples exhibited more pop-ins than H-A samples for particles II, III, and V, consistent with residual indents showing more SBs in L-R samples. Particle I presented an apparent contradiction: H-A samples had more pop-ins, but L-R samples showed denser SBs. This is attributed to high-density shear banding in L-R samples suppressing discrete pop-ins. Particle IV showed no pop-ins or obvious SBs in either sample, indicating a dominance of densification (a lower activation stress deformation mechanism) over shear flow. For particles I-III and V, more SBs in L-R samples meant a larger proportion of shear flow (which increases hardness) compared to H-A samples, explaining the modulus-hardness decoupling.

The remarkable 73.5% increase in Young's modulus of the H-A samples compared to L-R samples implied the extraordinary "ultra-stable" glass state It stems primarily from two hyper-aging-induced changes: significant volume shrinkage (10.8-12.5% per previous CE-5 studies) and extensive homogenization of elemental distribution [76]. Lunar glass's complex composition rich in O, Si, Fe, Mg, Al, and minor elements boasts high mixing entropy. Over eons of aging, this composition drives the material toward an "ultrastable glass state" with ultra-high density and minimal internal energy, eliminating atomic-scale defects and strengthening interatomic bonds. This unique natural prototype offers a robust design rationale for terrestrial ultra-stable glasses, targeting ultra-high modulus and superior irradiation resistance. For future lunar missions, its high modulus and structural stability make it a potential *in situ* construction material or protective coating for spacecraft components, withstanding extreme temperature swings and solar wind irradiation. More broadly, it inspires a new strategy for designing advanced amorphous materials: mimicking lunar hyper-aging via controlled long-term annealing or ion irradiation in laboratories, shortening the time to achieve the "ideal glass state" without sacrificing performance [56,77].

Geological significance of lunar glass

Lunar glass stands as an unparalleled "natural time capsule" of the Moon and inner solar system, encapsulating crucial evolutionary information in its morphology, chemical composition, formation age, and microstructure [45,68]. Unlike crystalline rocks that may undergo post-formation alteration, glass's amorphous structure locks in original signals, making it a reliable recorder of ancient lunar and solar system events. Its formation age serves as a core "geological clock" for reconstructing the Moon's evolutionary history, deciphering solar system impact dynamics, and even calibrating the chronology of other terrestrial planets [54]. Among dating techniques, radioisotope dating is the most mature and widely applied. Based on the decay patterns of radionuclides (e.g., $^{40}K \rightarrow {}^{40}Ar$, $^{238}U \rightarrow {}^{206}Pb$), it calculates age by measuring the ratio of parent to daughter nuclides [39,78]. There are two primary methods dominating lunar glass studies: $^{40}Ar/^{39}Ar$ dating and U-Pb dating.

$^{40}Ar/^{39}Ar$ dating hinges on the decay of ^{40}K to ^{40}Ar, a process uniquely suited to glass due to its ability to trap and retain argon during rapid quenching. Unlike crystalline minerals that may lose argon through thermal or tectonic activity, glass's dense atomic network preserves argon over billions of years. Age calculation is achieved via laser heating glass beads to release trapped argon, and mass spectrometry to measure the $^{40}Ar/^{39}Ar$ ratio, which correlates positively with formation age. Culler *et al.* emphasized that impact glass's chemical composition and age provide the most direct evidence for reconstructing the lunar impact history [58]. By applying this method to 155 glass beads from Apollo 14 lunar soil, researchers reconstructed regional and global lunar impact fluxes across different geological eras, revealing a striking "decline-surge" pattern [79]. Impact rates fell steadily for the first 2 billion years after the Moon's formation, then experienced unexpected surges, challenging the long-held view of a monotonically decreasing impact flux.

Uranium-lead (U-Pb) dating complements $^{40}Ar/^{39}Ar$ by targeting trace U and Pb in glass. During glass formation, intense melting volatilizes all original Pb, meaning any Pb detected later is solely the product of U decay ($^{238}U \rightarrow {}^{206}Pb$, $^{235}U \rightarrow {}^{207}Pb$). This "zero Pb" starting point makes U-Pb dating exceptionally precise. Long *et al.* applied this method to 215 impact glass spherules (50–200 μm in diameter) from CE-5 lunar regolith (Fig. 7a), a sample from one of the Moon's youngest regions [47]. Their results revealed ages spanning from millions to 2 billion years, with impact frequency showing multiple sharp peaks rather than a steady decline. Notably, one peak aligns with the 66-million-year-old Cretaceous-Paleogene boundary when dinosaurs went extinct. It confirms that lunar impacts and major Earth biological events may be driven by the same solar system impactor dynamics (e.g., comet showers or asteroid belt perturbations). These data provide critical "age anchors" for refining lunar crater chronology models, resolving the accuracy limitations of traditional crater counting [80–83].

Except for the above radioisotope dating, one novel kinetic dating method fills a longstanding gap: dating glass with extremely low isotope content, which is unsuitable for radiometric methods. Zhao *et al.* recently first systematically proposed this novel technique based on glass ultralow-ageing kinetics [84,85]. Its core principle is that glass's physical properties (e.g., enthalpy, elastic modulus) undergo predictable relaxation over time, following the KWW (Kohlrausch-Williams-Watts) relaxation function, as shown in Fig. 7b–d [86,87]. By measuring these property changes and establishing empirical correlations with effective relaxation time, temperature, and material brittleness, researchers can infer age without relying on isotopes (Fig. 7b, c). Zhao *et al.* tested this method on CE-5 lunar glass, obtaining ages of 86–161 million years, consistent with the U-Pb range of 2 million-2 billion years (Fig. 7d). Together, these three dating approaches create a comprehensive toolkit, spanning from ancient to young glass and from high to low isotope content. The combination of the current methods enables a

© Science China Press 2026

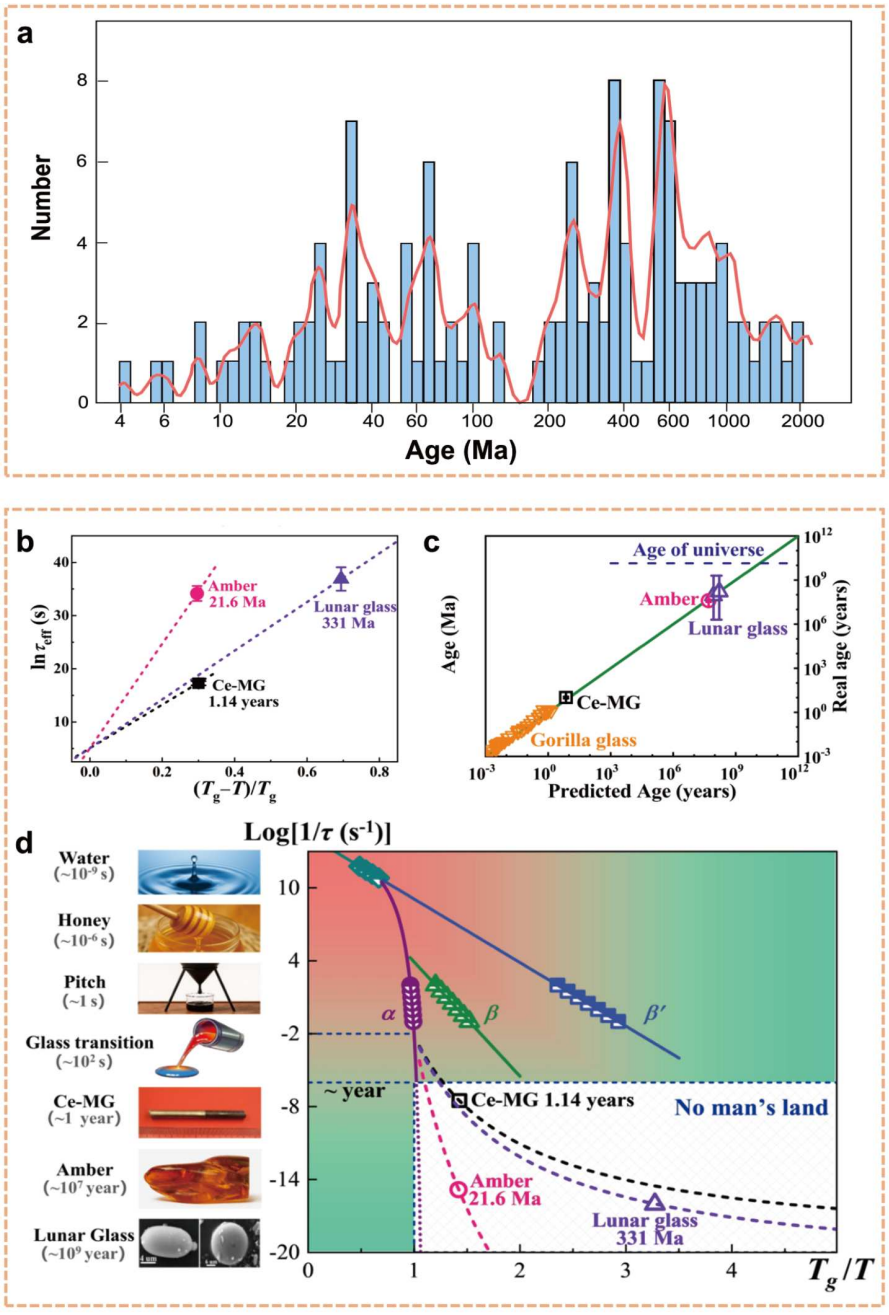

Figure 7 Geological dating and ultra-slow aging dynamics of impact glasses. (a) Age distribution of impact glass particles from CE-5 lunar soils determined by U-Pb isotope dating, reconstructing the impact history over the past ~2 Ga. Reprinted with permission from Ref. [47]. Copyright 2022, The American Association for the Advancement of Science. (b) Relationship between the effective relaxation time ln τ_{eff} and the normalized temperature parameter $(T_g - T)/T_g$ for amber, lunar glass, and metallic glass, with corresponding geological or experimental ages indicated; (c) Comparison between predicted dynamic ages derived from model inversion and independently constrained real ages for different glassy materials; (d) Unified diagram illustrating the relationship between relaxation time, temperature, and glass transition behavior, highlighting the ultra-slow aging regime and the so-called "no-man's land" in glass dynamics. Reprinted with permission from Ref. [84]. Copyright 2025, Springer Nature.

more precise and complete reconstruction of the Moon's geological history and the inner solar system's impact evolution.

STRATEGIC RESERVE DEPOT OF LUNAR RESOURCES

On Earth, glass has become an exceptional storage medium bridging natural and artificial environments due to its intrinsic structural stability, chemical inertness, and robust isolation capabilities [88]. Its storage value extends beyond mere "material preservation" to "information retention". Among natural glasses, amber formed by resin's rapid solidification, perfectly preserves ancient specimens from insects and reptiles to plant fragments for tens or even hundreds of millions of years (Fig. 8a, b) [89]. This not only preserves invaluable physical evidence for paleontology and paleoclimatology but also functions as a "natural archive" carrying ancient information.

© Science China Press 2026

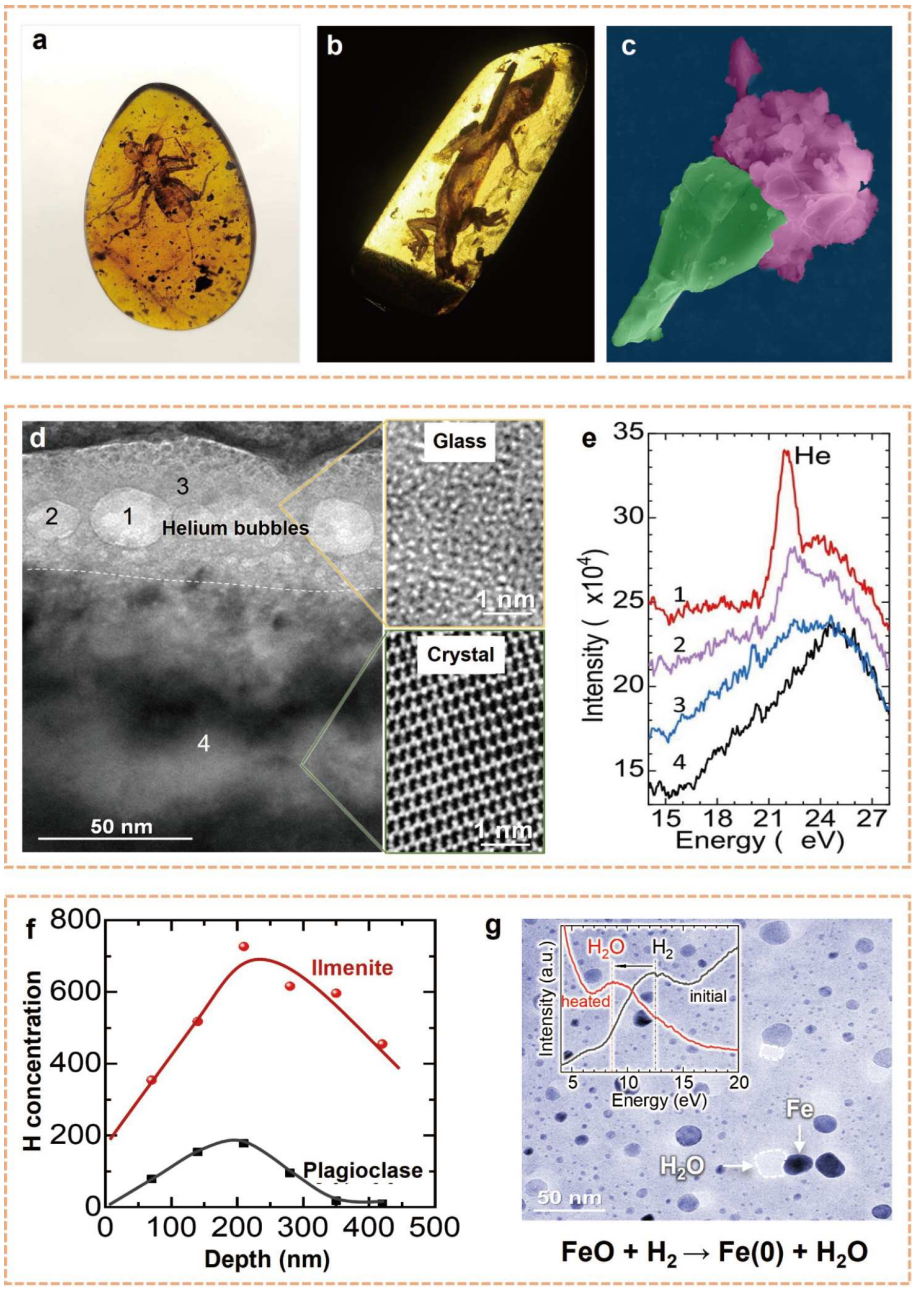

Figure 8 Trapping of solar-wind-derived volatiles and water formation associated with lunar glasses. (a, b) Representative images of biological inclusions preserved in natural amber, illustrating the long-term encapsulation capability of amorphous glassy materials on Earth. (c) A carnation flower like lunar particle composed of ilmenite ($FeTiO_3$, receptacle portion) and the agglutinates (corolla part). (d) TEM image showing helium bubbles trapped within a glassy coating on an ilmenite particle from CE-5 lunar soils; inset images highlight the amorphous glass matrix and adjacent crystalline regions; (e) Electron energy-loss spectroscopy (EELS) spectra acquired at different locations indicated in (d), confirming the presence and spatial variation of implanted helium. Reprinted with permission from Ref. [57]. Copyright 2022, IOP Publishing. (f) Depth profiles of H concentration in ilmenite and plagioclase grains from lunar soils, showing preferential H retention in ilmenite; (g) TEM image and schematic illustration of water formation during heating, involving the reduction of FeO by implanted H to produce metallic Fe^0 and H_2O within ilmenite-bearing lunar glass. Reprinted with permission from Ref. [90]. Copyright 2024, Elsevier.

In artificial applications, glass's versatility shines. High-purity quartz glass, with ultra-low gas permeability, stores specialty gases (noble gases, high-purity hydrogen) and nuclear waste, eliminating leakage risks [91]. Sealed glass containers shield cultural relics and biological samples (vaccines, cells) from oxygen, moisture, and microbial degradation [5,92]. Nanoscale glass microspheres precisely encapsulate drugs or catalysts for targeted release [93]. This all stems from glass's "long-range disorder, short-range order" amorphous structure devoid of grain boundary defects and chemically stable, it blocks external environmental interactions for long-term preservation [94]. Lunar glass inherits these terrestrial advantages and amplifies them via billions of years of extreme lunar conditions, which densify its structure and enhance inertness. This makes it a unique "strategic resource repository" on the Moon. The following parts will show three critical resources: solar wind-

© Science China Press 2026

implanted ^{3}He, trapped H and H_2O, each holding profound significance for future lunar exploration and *in situ* utilization.

Capturing ^{3}He resources

^{3}He is an ultra-safe, efficient, and clean nuclear fusion fuel, with enormous application potential for solving global energy crises. Yet its reserves on Earth are merely around 0.5 tons, extremely scarce [95,96]. In contrast, stellar fusion processes in space generate vast quantities of ^{3}He, which is continuously implanted into the lunar regolith by the solar wind due to the Moon's lack of an atmosphere. Investigating the distribution and abundance of ^{3}He on the Moon has thus become a core objective of the lunar exploration program [16,97].

Recently, Li *et al.* selected a particle composed of ilmenite ($FeTiO_3$) and agglutinates from Chang'e-5 lunar regolith (Fig. 8c) and studied the content of helium in these particles. They discovered that ilmenite particles feature a 40–50 nm thick amorphous glass layer on their surfaces, which is formed by long-term solar wind irradiation-induced amorphization [57]. Within this glass layer, numerous spherical helium bubbles (5–25 nm in diameter) were observed, mostly concentrated near the interface between the glass layer and the underlying crystalline matrix (Fig. 8d, e). Virtually no helium bubbles existed in the crystalline structure, as the ordered lattice has channeling effects that allow helium to escape. Further calculations revealed the helium atom number density in bubbles reaches 50–192 He/nm^3, corresponding to internal pressures of 1–39 GPa. Based on lunar ilmenite reserves and the ^{3}He/^{4}He ratio of ~4×10^{-4}, the total ^{3}He stored in such bubbles is estimated to reach 260,000 tons. The amorphous glass layer acts as a unique "trapping and storage carrier" for solar wind-injected helium. Helium atoms first implant into the ilmenite lattice via solar wind, then diffuse outward through lattice channels. The glass layer's disordered atomic packing lacks fixed diffusion pathways, effectively blocking helium migration and restricting its release. Over time, the trapped helium accumulates to form high-pressure bubbles, with Fe-rich nano-clusters surrounding bubbles potentially aiding stabilization.

Crucially, previous studies have suggested that ^{3}He is dissolved in lunar regolith particles, and its extraction is limited by diffusion rates, requiring high temperatures above 700 °C [16,97]. This approach not only entails high energy consumption but also low efficiency, making it unfeasible for *in situ* mining on the Moon. In contrast, ^{3}He existing in the form of bubbles is expected to be extracted at room temperature via mechanical crushing without high-temperature heating. Furthermore, ilmenite exhibits weak magnetism and can be separated from other lunar regolith particles through magnetic separation, which facilitates *in situ* mining on the Moon [98–102]. This drastically reduces energy consumption for *in situ* utilization. If fully harnessed for nuclear fusion, this ^{3}He reserve could satisfy global energy demands for 2600 years. These findings not only clarify the enrichment mechanism of lunar ^{3}He but also lay a solid theoretical foundation for future low-cost *in situ* extraction, opening a practical pathway to exploit lunar energy resources for human sustainable development.

Capturing H resources and producing water

Hydrogen is the linchpin of sustainable lunar exploration, as it is the core feedstock for *in situ* water production, essential for human survival, oxygen generation, and energy supply on the Moon. Yet the lunar surface is extremely scarce in natural water and hydroxyl (OH), with concentrations only ranging from 10 to 1000 ppm, far from meeting practical demands. While the solar wind continuously implants H into lunar regolith, this endogenous H is highly mobile and prone to escaping through the ordered lattice channels of crystalline minerals, making effective capture and utilization a long-standing challenge. This bottleneck was broken by the groundbreaking research, which revealed that lunar ilmenite coupled with its associated glassy phases acts as a natural "H trap" to unlock large-scale H_2O production [90].

Notably, Chen *et al.* [90] recently proposed for the first time that ilmenite ($FeTiO_3$) in CE-5 lunar soil can react with this solar wind-implanted endogenous H to generate water at scale. Among CE-5 regolith's components (44.5 wt.% pyroxene, 30.4 wt.% plagioclase, 15.5 wt.% glasses, 6.0 wt.% ilmenite, 3.6 wt.% olivine [16]), ilmenite stands out with the strongest H-storage capacity. Its unique sub-nanometer tunnel-like crystal structure locks in H atoms, while the glassy layer coating its surface (a product of long-term solar wind bombardment) blocks further diffusion, creating an ideal H-trapping environment. EELS analysis (pinpointing H via a 12.5 eV peak) reveals only ilmenite and plagioclase hold detectable H [90]. Pyroxene and olivine have negligible levels, likely due to their more open lattices that let H escape. Ilmenite's H concentration is roughly four times that of plagioclase, a difference vividly shown in Fig. 8f. For ilmenite (red curve), H surges with depth, peaks around 200 nm (where the glassy layer interfaces with the crystal core), and stays high even at 500 nm. In contrast, plagioclase (black curve), by contrast, sees a mild H rise to a shallow peak, then drops to near zero by 400 nm. The above results obviously show that proving ilmenite's superior H retention at greater depths due to its glass-crystal structure.

Hydrogen stored in ilmenite acts as a potent reducing agent. When regolith is heated above 1200 K (its melting point, achievable via *in situ* solar thermal systems), H reacts with iron oxides: $FeO + 2H \rightarrow Fe + H_2O$; $Fe_2O_3 + 6H \rightarrow 2Fe + 3H_2O$. High-magnification TEM images (Fig. 8g) capture this in real time: dark Fe nanocrystals and bright H_2O bubbles form side-by-side, confirming the reaction's mechanism. Chen *et al.* confirmed that one gram of lunar regolith can yield approximately 51–76 mg of H_2O. Based on this calculation, one ton of lunar regolith could produce about 50–70 kg of H_2O. This is equivalent to over 100 bottles of 500 mL bottled water, which is essentially sufficient to meet the daily drinking water needs of 50 people. Moreover, the produced H_2O can also be electrolyzed into H_2 and O_2, powering base systems and refueling spacecraft. These findings turn regolith into a viable resource depot, laying groundwork for long-term lunar habitation.

The natural water content of lunar regolith as a whole is extremely low (only 0.0001 wt%–0.02 wt%; for example, the water content of CE-5 samples is a mere 180 ppm) [103,104]. Faced with such trace water content, existing extraction technologies generally suffer from low extraction efficiency and excessively high energy and operational costs, which render them unable to support large-scale mining. Meanwhile, although molecular water-bearing minerals with a water content of up to 41 wt% have been identified in lunar regolith, their abundance in lunar regolith is extremely low [103]. Current technologies lack efficient and targeted enrichment methods for such minerals, failing to effectively utilize these high-water-content minerals

© Science China Press 2026

and thus further limiting the actual recoverable amount of water from lunar regolith.

Capturing water resources

Water is the lifeline of lunar exploration: it quenches astronaut thirst, splits into oxygen for breathing, and synthesizes rocket fuel, eliminating the need to haul heavy supplies from Earth. Yet for decades, the Moon was labeled a "dry desert": no atmosphere to trap moisture, and extreme diurnal temperatures that seemed to banish liquid water. This dryness once loomed as the biggest barrier to long-term lunar habitation until studies of lunar glass uncovered a hidden "water warehouse", rewriting our understanding of the Moon's resources.

Saal *et al.* provided crucial evidence for lunar glass's water storage properties and water origins via *in situ* analysis of Apollo 15 and 17 lunar volcanic glass and olivine melt inclusions [44]. Before this work, the research community widely assumed the Moon's interior was bone-dry, but their focus on H, H_2O, OH content and isotopic traits. Fig. 9a, b revealed widespread dissolved water in these samples. Olivine melt inclusions, sealed tight within crystals, escaped degassing during volcanic eruptions, preserving pristine magmatic water with H_2O concentrations up to 1200 ppm. In contrast, the surrounding matrix glass exposed to space during eruption lost most moisture to degassing, containing just 3–32 ppm H_2O. This proved lunar glass (especially well-enclosed grains or inclusions) has a robust capacity to capture and seal water.

Liu *et al.* expanded this insight by studying Apollo samples: they found abundant hydroxyl groups in impact-formed cemented glass, tracing them to solar wind H injection [105].

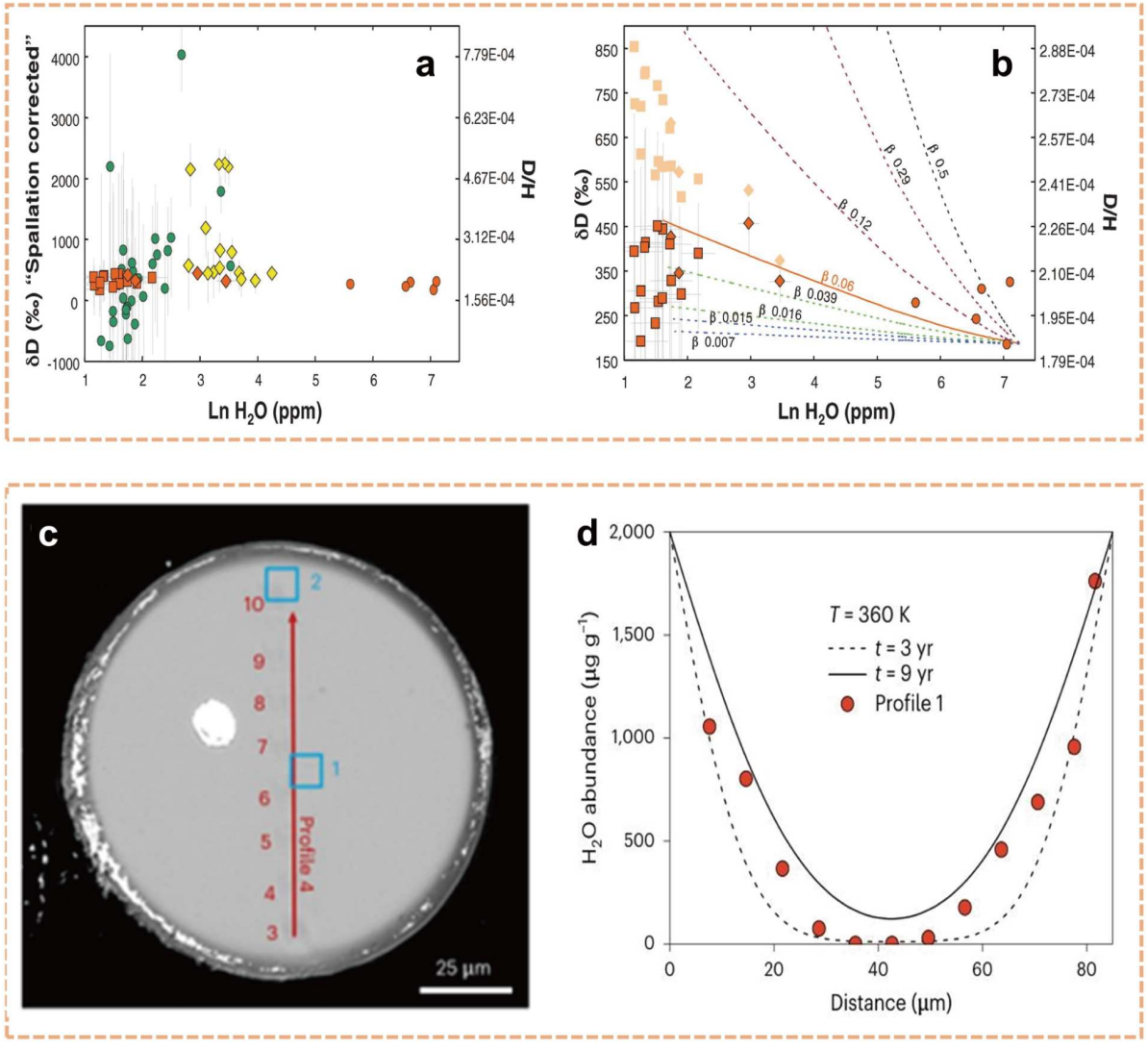

Figure 9 H_2O contents and H isotope compositions of lunar volcanic glasses and melt inclusions. (a) Relationship between water content (ln H_2O, ppm) and H isotopic composition (δD, ‰), corrected for cosmic-ray spallation effects, for very-low-Ti glasses, low-Ti glasses, and high-Ti melt inclusions, matrix glasses, and glass beads; (b) Comparison of spallation-corrected and uncorrected H isotope data for high-Ti glasses and melt inclusions, together with model curves representing diffusive degassing of H_2, H_2O, and OH^-. Reprinted with permission from Ref. [39]. Copyright 2013, American Association for the Advancement of Science. (c) SEM image of a cross-sectioned impact glass bead, showing the location of the analytical transect (profile 1); (d) Water concentration profile measured along profile 1 in (c), revealing elevated water contents near the bead surface; model curves illustrate diffusion profiles corresponding to different residence times. Reprinted with permission from Ref. [105]. Copyright 2023, Springer Nature.

© Science China Press 2026

Pioneering CE-5 impact glass bead studies have now elevated this understanding. These beads hold significant water, with a clear concentration gradient (Fig. 9c, d) that drops from the particle edge to the center. This result provides direct evidence that solar wind H atoms implant at the surface and diffuse inward, making the beads a critical, previously underappreciated reservoir for solar wind-derived water. Estimates suggest lunar glass stores up to 2.7×10^{14} kilograms of water, a scale large enough to sustain long-term lunar base operations.

The estimation of H_2O and ^3He reserves hosted in lunar glass is subject to multiple critical uncertainties. Spatial heterogeneity results in substantial variations in volatile concentrations and occurrence patterns across different lunar geological units. However, current observational and sample data are limited to a small number of landing sites, which cannot represent the full range of lunar geological contexts. Moreover, the influences of particle size on H_2O adsorption and ^3He implantation processes remain underexplored, and the particle size distribution of lunar glass samples has not been sufficiently characterized. Meanwhile, the restricted sampling coverage of lunar missions introduces significant sampling biases, which fail to reflect the global distribution characteristics of lunar glass. Collectively, these interconnected factors impose severe constraints on the accuracy and reliability of reserve estimation.

From terrestrial amber to lunar glass, glass materials' storage properties do not just persist, but they strengthen in extreme celestial environments. Lunar glass is not terrestrial glass's cosmic copy. Forged by impact melt quenching, it evolved under the Moon's vacuum, solar radiation, and 310 K diurnal swings, honing its ability to lock in ^3He, H and H_2O. Naturally formed, resource-dense, and extraterrestrial-adapted, it is a core target for ISRU, laying not just lunar base groundwork, but a blueprint for sustaining deep-space exploration to Mars and beyond.

DEVELOPING NOVEL AMORPHOUS SOFT MAGNETIC ALLOY INSPIRED FROM LUNAR GLASS

Billions of years of solar wind bombardment infuses substantial amounts of H into lunar materials, with lunar glass serving as a key reservoir for this implanted element. This trapped H plays a pivotal role in fostering the growth of Fe clusters within the glass matrix. When heated to elevated temperatures, the stored H is released and engages in chemical reactions with the glass, ultimately yielding Fe nanocrystals, a process shaped by the unique space environment (Fig. 5c–g). A striking contrast emerges between the crystallization behaviors of the solar wind-irradiated surface layer and the unirradiated interior: the irradiated region sees a significant reduction in crystallization onset temperature, leading to the formation of denser, more uniformly distributed nanocrystals embedded in the amorphous base.

These natural observations offer profound inspiration for engineering nanocrystalline/amorphous alloys, particularly Fe-based amorphous alloys. Enhancing the soft magnetic properties of these alloys relies heavily on controlled crystallization that produces fine and homogeneous Fe nanocrystals. For now, it is still a core challenge in advancing high-performance soft magnetic materials. To replicate the solar wind's effect, Chen *et al.* turned to H^+ irradiation by selecting $Fe_{88}B_{14}$ (FeB) amorphous alloy as a model due to its potential as a premium nanocrystalline precursor [71]. The pristine FeB sample exhibits a classic amorphous structure with no detectable short-range ordered clusters (Fig. 10a), and its crystallization results in relatively large nanocrystals that compromise soft magnetic performance (Fig. 10b, e). In stark contrast, H^+ irradiation creates a thin (~10 nm) surface layer (Fig. 10c). This surface layer retains an amorphous structure but features stronger structural fluctuations and distinct contrast clusters, mirroring the irradiated layer of lunar glass. After crystallization, the nanocrystals in this modified layer measure just 5–8 nm, far smaller than the 15–20 nm grains in the unirradiated interior (Fig. 10d, f). This refined microstructure translates to tangible performance gains: at 10 kHz, the irradiated FeB's relative permeability reaches 1442, a 10.2% improvement over the unirradiated sample's 1308 (Fig. 10g).

The findings demonstrate that H^+ irradiation serves as a robust tool for tailoring the crystallization behavior of Fe-based metallic glasses. Beyond enabling the formation of nanocrystals with a fine, highly uniform distribution, this irradiation strategy notably reduces the crystallization onset temperature within the treated surface layer. This key attribute expands the annealing temperature window for fabricating nanocrystalline soft magnetic materials, creating more flexibility in processing and further fostering the development of a homogeneous nanocrystal arrangement [28,37,106,107]. Yet, a critical constraint persists: the influence of H^+ irradiation is confined to the material's surface, typically penetrating only a few tens of nanometers deep. As such, a central challenge for future research lies in extending this irradiation-induced modification to the bulk of the material, rather than limiting it to superficial layers. Nevertheless, despite this limitation, the results open up a promising pathway for enhancing the soft magnetic properties of Fe-based metallic glasses. By precisely controlling their nanocrystallization process through this irradiation technique, researchers gain a viable method to optimize the performance of these advanced materials for practical applications.

CONCLUSIONS AND OUTLOOK

In conclusion, this review systematically summarizes the multidisciplinary value of lunar glass, spanning planetary science, resource engineering, and materials science. It covers lunar glasses' diverse formation pathways, unique physical properties, critical geological significance, substantial resource potential, and profound implications for advanced material design. By bridging extraterrestrial natural amorphous materials with terrestrial artificial material innovation, this work lays a foundation for integrating lunar exploration with technological application.

With the advancement of China's CE lunar exploration program and the global push for crewed lunar missions, research on lunar glass is shifting from basic compositional characterization to probing extreme physical origins and expanding engineering applications. Future research will focus on three cutting-edge directions.

Searching for "ideal glass". The nature of the glassy state, particularly the physical mechanism of the glass transition, remains a major unsolved puzzle in condensed matter physics [108]. Terrestrial synthetic glasses constrained by human timescales and experimental windows, are trapped in high-energy non-equilibrium states, making it difficult to reach the theoretically predicted low-energy "Ideal Glass" state. Lunar glass, however, offers a solution. CE-5's young samples and Apollo's ancient glass beads have undergone millions to billions of years of natural ultra-aging, asymptotically approaching the thermodynamic Kauzmann Point. Future research should employ high-

© Science China Press 2026

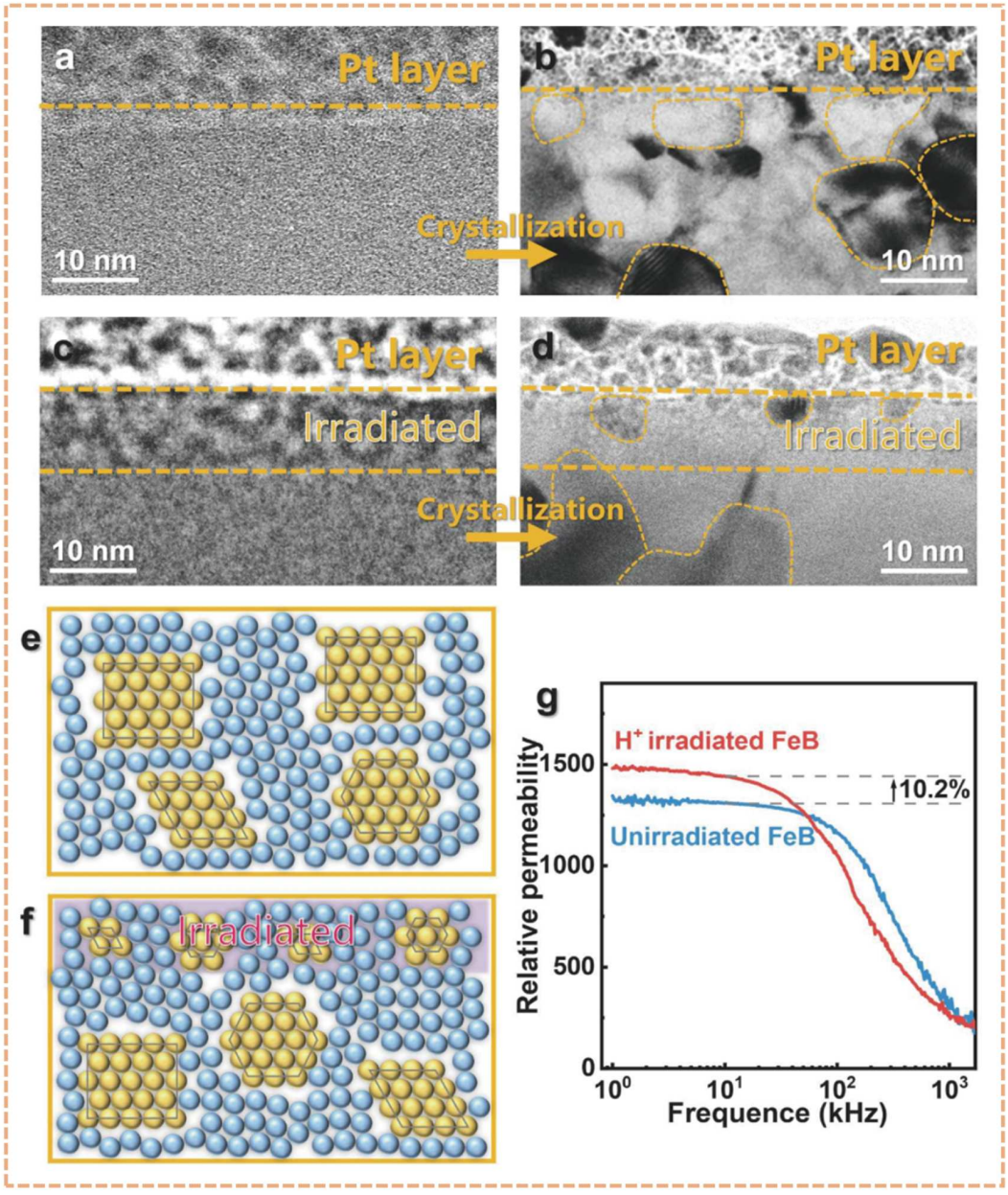

Figure 10 Ion-irradiation-regulated crystallization behavior and magnetic properties of FeB metallic glass. (a, b) HRTEM images of unirradiated FeB metallic glass before and after crystallization, respectively, showing the formation of relatively coarse and heterogeneous nanocrystals; (c, d) HRTEM images of ion-irradiated FeB metallic glass before and after crystallization, revealing refined and more uniformly distributed nanocrystals; (e, f) Schematic illustrations summarizing the distinct crystallization pathways in unirradiated and irradiated FeB metallic glasses; (g) Frequency dependence of relative permeability for crystallized FeB metallic glass with and without ion irradiation, demonstrating enhanced magnetic performance after irradiation-induced nano-structural refinement. Reprinted with permission from Ref. [71]. Copyright 2025, Springer Nature.

precision calorimetry and synchrotron radiation techniques to analyze residual entropy and atomic packing density in lunar glass across different geological ages and to test the existence of the ultrastable "Ideal Glass" phase. This will not only challenge traditional understandings of glass transitions but also guide the development of terrestrial amorphous materials with exceptional kinetic stability. It should be noted that the interpretation of "ideal glass" and the approach toward the Kauzmann limit remains hypothesis-driven and speculative. Direct experimental verification of this theoretical inference remains challenging due to the inability to replicate the billion-year natural aging of lunar glass in laboratory settings.

Decoding low-temperature relaxation mechanisms. The Moon's extreme diurnal temperature swings (–180 °C to +130 °C) create a natural laboratory for studying low-temperature thermal cycling effects. Future research must focus on the cumulative impacts of low-temperature relaxation over geological timescales and the related critical issues. For example, how atomic clusters in lunar glass dissipate energy through secondary relaxation driven by hundreds of millions of thermal cycles? Or

© Science China Press 2026

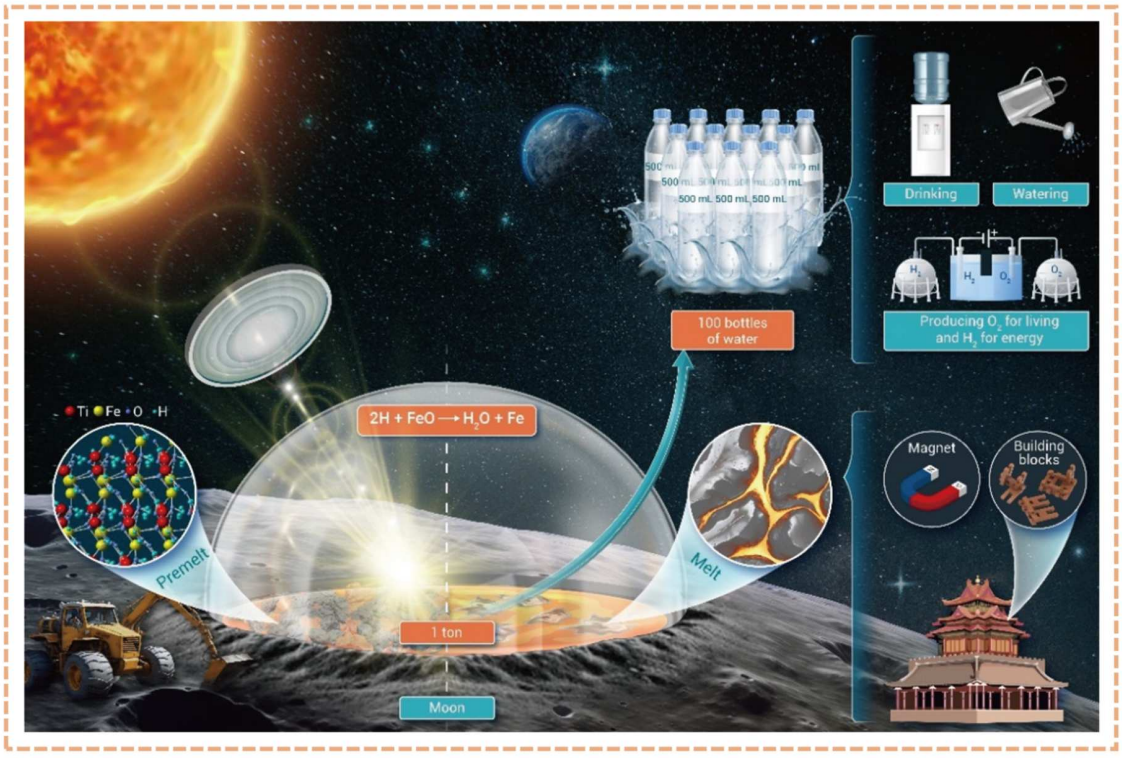

Figure 11 Schematic illustration of on-site H_2O production on the Moon. Lunar regolith-derived glass is proposed to be fabricated into optical components, such as lenses, to concentrate solar radiation and serve as a heating element in *in situ* resource utilization (ISRU) systems. Concentrated solar energy enables thermal processing of lunar materials, facilitating the release and generation of water, thereby highlighting the functional importance of lunar glass in extraterrestrial resource utilization. Reprinted with permission from Ref. [90]. Copyright 2024, Elsevier.

whether this unique relaxation mode endows lunar glass with exceptional mechanical toughness or radiation resistance? Elucidating this mechanism will not only refine structural relaxation-based dating models for lunar materials but also provide critical physical frameworks for understanding atomic motion in amorphous solids under ultra-long-term and extreme temperature coupling. The related researches will fill a key gap in terrestrial materials science regarding the key behavior under coupled fields of ultra-long periods and extreme temperature fluctuations.

Developing ISRU technology. While lunar glass's capacity to trap solar wind-derived water and ^{3}He is well confirmed, achieving low-energy, high-efficiency "non-destructive extraction" remains a critical engineering bottleneck for ISRU. As visualized in Fig. 11, the ISRU chain unfolds vividly: a single ton of lunar regolith (excavated via the rover-equipped excavator in the scene) can be processed to unlock hidden resources. It is driven by the reaction 2H + FeO → H_2O + Fe triggered during controlled melting of the material. While lunar glass's ability to trap solar wind-derived water and ^{3}He is already well confirmed, translating this potential into low-energy, high-efficiency "non-destructive extraction" remains the critical engineering bottleneck holding back practical ISRU. Future research must move beyond mere resource abundance quantification to delve into gas and water diffusion kinetics within the glass network. Specifically, how unique microstructures like helium bubbles, solar wind-induced irradiation layers and nanoclusters regulate mass transport within the lunar regolith? Efforts should focus on developing targeted technologies: thermal release protocols leveraging glass's high T_g and broad supercooled liquid region, or microwave-assisted extraction tailored to its amorphous structure. These innovations will deliver actionable solutions for on-site acquisition of life-support and energy resources, laying the groundwork for self-sustaining lunar bases and advancing deep-space exploration toward true resource independence.

Received 12 January 2026; accepted 27 February 2026; published online 4 June 2026

1 Shelby JE. Introduction to Glass Science and Technology. London: The Royal Society of Chemistry, 2005
2 Boon S. Glass act. Nature, 2019, 575: 250
3 Spinella L, Uličná S, Sinha A, *et al.* Chemical and mechanical interfacial degradation in bifacial glass/glass and glass/transparent backsheet photovoltaic modules. Prog Photovoltaics, 2022, 30: 1423–1432
4 Dengale SJ, Grohganz H, Rades T, *et al.* Recent advances in co-amorphous drug formulations. Adv Drug Deliver Rev, 2016, 100: 116–125
5 Fang MA, Ming-Fang C, Jian-Hua Z, *et al.* Porous hydroxyapatite microspheres prepared by using poly (allylamine hydrochloride) and its application in drug delivery. J InOrg Mater, 2017, 32: 1215
6 Yu L. Amorphous pharmaceutical solids: Preparation, characterization and stabilization. Adv Drug Deliver Rev, 2001, 48: 27–42
7 Hancock BC, Zografi G. Characteristics and significance of the amorphous state in pharmaceutical systems. J Pharm Sci, 1997, 86: 1–12
8 Blaabjerg LI, Lindenberg E, Löbmann K, *et al.* Glass forming ability of amorphous drugs investigated by continuous cooling and isothermal transformation. Mol Pharm, 2016, 13: 3318–3325
9 Eggleton BJ, Luther-Davies B, Richardson K. Chalcogenide photonics.

© Science China Press 2026

Nat Photon, 2011, 5: 141–148
10 Carlson DE, Wronski CR. Amorphous silicon solar cell. Appl Phys Lett, 1976, 28: 671–673
11 Sohrabi S, Fu J, Li L, *et al.* Manufacturing of metallic glass components: processes, structures and properties. Prog Mater Sci, 2024, 144: 101283
12 Bennett TD, Tan JC, Yue Y, *et al.* Hybrid glasses from strong and fragile metal-organic framework liquids. Nat Commun, 2015, 6: 8079
13 Klement Jun. W, Willens RH, Duwez P. Non-crystalline structure in solidified gold-silicon alloys. Nature, 1960, 187: 869–870
14 Xu D, Pan C. Glass formation, structure, relaxation, and property of metal-organic framework (MOF) glasses: a review. Prog Nat Sci-Mater Int, 2025, 35: 98–121
15 Zellner NEB. Lunar impact glasses: probing the moon's surface and constraining its impact history. JGR Planets, 2019, 124: 2686–2702
16 Li C, Hu H, Yang MF, *et al.* Characteristics of the lunar samples returned by the Chang'e-5 mission. Natl Sci Rev, 2022, 9: nwab188
17 Tarduno JA, Cottrell RD, Lawrence K, *et al.* Absence of a long-lived lunar paleomagnetosphere. Sci Adv, 2021, 7: eabi7647
18 Keller LP, McKay DS. Discovery of vapor deposits in the lunar regolith. Science, 1993, 261: 1305–1307
19 Noguchi T, Nakamura T, Kimura M, *et al.* Incipient space weathering observed on the surface of Itokawa dust particles. Science, 2011, 333: 1121–1125
20 Fredriksson K, Nelen J, Melson WG, *et al.* Lunar glasses and microbreccias: properties and origin. Science, 1970, 167: 664–666
21 Hu X, Jiang T, Ma P, *et al.* A spectral library study of mixtures of common lunar minerals and glass. Remote Sens, 2023, 15: 2195
22 Tian HC, Wang H, Chen Y, *et al.* Non-KREEP origin for Chang'e-5 basalts in the Procellarum KREEP Terrane. Nature, 2021, 600: 59–63
23 Hiroi T, Abe M, Kitazato K, *et al.* Developing space weathering on the asteroid 25143 Itokawa. Nature, 2006, 443: 56–58
24 Wetzel DT, Hauri EH, Saal AE, *et al.* Carbon content and degassing history of the lunar volcanic glasses. Nat Geosci, 2015, 8: 755–758
25 Li C, Ma W, Li Y, *et al.* Metallurgical performance evaluation of space-weathered Chang'e-5 lunar soil. Int J Miner Metall Mater, 2024, 31: 1241–1248
26 Wang BW, Zhang QWL, Chen Y, *et al.* Returned samples indicate volcanism on the Moon 120 million years ago. Science, 2024, 385: 1077–1080
27 Zeigler RA, Korotev RL, Jolliff BL, *et al.* The geochemistry and provenance of Apollo 16 mafic glasses. Geochim Cosmochim Acta, 2006, 70: 6050–6067
28 Starukhina LV. Polar regions of the moon as a potential repository of solar-wind-implanted gases. Adv Space Res, 2006, 37: 50–58
29 Taylor LA, Pieters C, Keller LP, *et al.* The effects of space weathering on Apollo 17 mare soils: petrographie and chemical characterization. Meteorit Planet Scien, 2001, 36: 285–299
30 Burgess KD, Stroud RM. Phase-dependent space weathering effects and spectroscopic identification of retained helium in a lunar soil grain. Geochim Cosmochim Acta, 2018, 224: 64–79
31 Li S, Milliken RE. Water on the surface of the Moon as seen by the Moon Mineralogy Mapper: distribution, abundance, and origins. Sci Adv, 2017, 3: e1701471
32 Zhou C, Tang H, Li X, *et al.* Chang'e-5 samples reveal high water content in lunar minerals. Nat Commun, 2022, 13: 5336
33 Xu Y, Tian HC, Zhang C, *et al.* High abundance of solar wind-derived water in lunar soils from the middle latitude. Proc Natl Acad Sci USA, 2022, 119: e2214395119
34 Zhang H, Zhang X, Zhang G, *et al.* Size, morphology, and composition of lunar samples returned by Chang'e-5 mission. Sci China-Phys Mech Astron, 2022, 65: 229511
35 Cao H, Wang C, Chen J, *et al.* A Raman spectroscopic and microimage analysis perspective of the Chang'e-5 lunar samples. Geophys Res Lett, 2022, 49: e2022GL099282
36 Xiao Z, Yan P, Wu B, *et al.* Translucent glass globules on the Moon. Sci Bull, 2022, 67: 355–358
37 Pieters CM, Goswami JN, Clark RN, *et al.* Character and spatial distribution of OH/H_2O on the surface of the Moon seen by M^3 on Chandrayaan-1. Science, 2009, 326: 568–572
38 Vernazza P, Binzel RP, Rossi A, *et al.* Solar wind as the origin of rapid reddening of asteroid surfaces. Nature, 2009, 458: 993–995
39 Saal AE, Hauri EH, Van Orman JA, *et al.* Hydrogen isotopes in lunar volcanic glasses and melt inclusions reveal a carbonaceous chondrite heritage. Science, 2013, 340: 1317–1320
40 Guo JG, Ying T, Gao H, *et al.* Surface microstructures of lunar soil returned by Chang'e-5 mission reveal an intermediate stage in space weathering process. Sci Bull, 2022, 67: 1696–1701
41 Guo ZS, Xing D, Xi XY, *et al.* Production of fibres from lunar soil: feasibility, applicability and future perspectives. Adv Fiber Mater, 2022, 4: 923–937
42 Delano JW. Pristine lunar glasses: criteria, data, and implications. J Geophys Res, 1986, 91: 201–213
43 Hui H, Hess KU, Zhang Y, *et al.* Cooling rates of lunar orange glass beads. Earth Planet Sci Lett, 2018, 503: 88–94
44 Saal AE, Hauri EH, Cascio ML, *et al.* Volatile content of lunar volcanic glasses and the presence of water in the Moon's interior. Nature, 2008, 454: 192–195
45 Zhao R, Shen L, Xiao D, *et al.* Diverse glasses revealed from Chang'e-5 lunar regolith. Natl Sci Rev, 2023, 10: nwad079
46 Husain L, Schaeffer OA. Lunar volcanism: age of the glass in the Apollo 17 orange soil. Science, 1973, 180: 1358–1360
47 Long T, Qian Y, Norman MD, *et al.* Constraining the formation and transport of lunar impact glasses using the ages and chemical compositions of Chang'e-5 glass beads. Sci Adv, 2022, 8: eabq2542
48 Zhao R, Shen L, Chao C, *et al.* Lunar glass. Acta Phys Sin, 2023, 72: 236101
49 Pieters CM, Taylor LA, Noble SK, *et al.* Space weathering on airless bodies: resolving a mystery with lunar samples. Meteorit Planet Scien, 2000, 35: 1101–1107
50 Naser MZ. Extraterrestrial construction materials. Prog Mater Sci, 2019, 105: 100577
51 Hapke B. Space weathering from Mercury to the asteroid belt. J Geophys Res, 2001, 106: 10039–10073
52 Pieters CM, Noble SK. Space weathering on airless bodies. JGR Planets, 2016, 121: 1865–1884
53 Yang W, Chen Y, Wang H, *et al.* Geochemistry of impact glasses in the Chang'e-5 regolith: constraints on impact melting and the petrogenesis of local basalt. Geochim Cosmochim Acta, 2022, 335: 183–196
54 Cao K, Dong M, She Z, *et al.* A novel method for simultaneous analysis of particle size and mineralogy for Chang'e-5 lunar soil with minimum sample consumption. Sci China Earth Sci, 2022, 65: 1704–1714
55 Pieters CM, Ammannito E, Blewett DT, *et al.* Distinctive space weathering on Vesta from regolith mixing processes. Nature, 2012, 491: 79–82
56 Keller LP, McKay DS. The nature and origin of rims on lunar soil grains. Geochim Cosmochim Acta, 1997, 61: 2331–2341
57 Li A, Chen X, Song L, *et al.* Taking advantage of glass: capturing and retaining the helium gas on the moon. Mater Futures, 2022, 1: 035101
58 Nguyen P, Zellner N. Using size and composition to assess the quality of lunar impact glass ages. Geosciences, 2019, 9: 85
59 Guo Z, Li Y, Chen H, *et al.* Evidence for the disproportionation of iron in a eucrite meteorite: implications for impact processes on Vesta. JGR Planets, 2021, 126: e2020JE006816
60 Bindi L, Shim SH, Sharp TG, *et al.* Evidence for the charge disproportionation of iron in extraterrestrial bridgmanite. Sci Adv, 2020, 6: eaay7893
61 Guo Z, Li Y, Liu S, *et al.* Discovery of nanophase iron particles and high pressure clinoenstatite in a heavily shocked ordinary chondrite: implications for the decomposition of pyroxene. Geochim Cosmochim Acta, 2020, 272: 276–286
62 Cannon KM, Mustard JF, Parman SW, *et al.* Spectral properties of Martian and other planetary glasses and their detection in remotely sensed data. JGR Planets, 2017, 122: 249–268
63 Xian H, Zhu J, Yang Y, *et al.* Ubiquitous and progressively increasing ferric iron content on the lunar surfaces revealed by the Chang'e-5 sample. Nat Astron, 2023, 7: 280–286

© Science China Press 2026

64 Li C, Guo Z, Li Y, *et al*. Impact-driven disproportionation origin of nanophase iron particles in Chang'e-5 lunar soil sample. Nat Astron, 2022, 6: 1156–1162
65 Sasaki S, Nakamura K, Hamabe Y, *et al*. Production of iron nanoparticles by laser irradiation in a simulation of lunar-like space weathering. Nature, 2001, 410: 555–557
66 Lucey PG. A lunar waterworld. Science, 2009, 326: 531–532
67 Shearer CK, Papike JJ, Galbreath KC, *et al*. A SIMS study of lunar "komatiitic glasses": trace element characteristics and possible origin. Geochim Cosmochim Acta, 1990, 54: 1851–1857
68 Yan P, Xiao Z, Wu Y, *et al*. Intricate regolith reworking processes revealed by microstructures on lunar impact glasses. JGR Planets, 2022, 127: e2022JE007260
69 Yan P, Xiao Z, Wu Y, *et al*. Adhesion of silicate impact melts on impact glasses of Chang'e-5 regolith. JGR Planets, 2024, 129: e2024JE008777
70 Yan P, Xiao Z, Wu Y, *et al*. Submicroscopic iron-rich grains throughout impact glasses in Chang'e-5 regolith. Icarus, 2024, 410: 115920
71 Chen X, Ma B, Song L, *et al*. From lunar glass to advanced metallic glass: dense nanocrystallization catalyzed by implanted ions. Sci China Mater, 2025, 68: 2433–2441
72 Wang WH. Dynamic relaxations and relaxation-property relationships in metallic glasses. Prog Mater Sci, 2019, 106: 100561
73 Mauro JC. Decoding the glass genome. Curr Opin Solid State Mater Sci, 2018, 22: 58–64
74 Gulbiten O, Mauro JC, Guo X, *et al*. Viscous flow of medieval cathedral glass. J Am Ceram Soc, 2018, 101: 5–11
75 Wang Y, Zhang K, Feng Y, *et al*. Excellent irradiation tolerance and mechanical behaviors in high-entropy metallic glasses. J Nucl Mater, 2019, 527: 151785
76 Chen Z, Zhao Y, Chi X, *et al*. Geological timescales' aging effects of lunar glasses. Sci Adv, 2023, 9: eadi6086
77 Norman MD, Jourdan F, Hui SSM. Impact history and regolith evolution on the moon: geochemistry and ages of glasses from the Apollo 16 site. JGR Planets, 2019, 124: 3167–3180
78 Saal AE, Hauri EH. Large sulfur isotope fractionation in lunar volcanic glasses reveals the magmatic differentiation and degassing of the Moon. Sci Adv, 2021, 7: eabe4641
79 Culler TS, Becker TA, Muller RA, *et al*. Lunar impact history from $^{40}Ar/^{39}Ar$ dating of glass spherules. Science, 2000, 287: 1785–1788
80 Zhang L, Wang P, Chen XY, *et al*. Review in detrital zircon U-Pb geochronology: data acquisition, analysis and comparison. Adv Earth Sci, 2020, 35: 414–430
81 Nemchin AA, Norman MD, Grange ML, *et al*. U-Pb isotope systematics and impact ages recorded by a chemically diverse population of glasses from an Apollo 14 lunar soil. Geochim Cosmochim Acta, 2022, 321: 206–243
82 Melosh HJ, Vickery AM. Melt droplet formation in energetic impact events. Nature, 1991, 350: 494–497
83 Johnson B. The Formation of Distal Impact Ejecta. Dissertation for Doctoral Degree. West Lafayette: Purdue University, 2013
84 Zhao Y, Zhang H, Xu L, *et al*. Ultra-slow aging dynamics of glass and its application to geological dating. Nat Commun, 2025, 16: 11631
85 Vaknin A, Ovadyahu Z, Pollak M. Aging effects in an anderson insulator. Phys Rev Lett, 2000, 84: 3402–3405
86 Dyre JC. Narayanaswamy's 1971 aging theory and material time. J Chem Phys, 2015, 143: 114507
87 Phillips JC. Stretched exponential relaxation in molecular and electronic glasses. Rep Prog Phys, 1996, 59: 1133–1207
88 Conradt R. Chemical durability of oxide glasses in aqueous solutions: a review. J Am Ceramic Soc, 2008, 91: 728–735
89 Shi G, Grimaldi DA, Harlow GE, *et al*. Age constraint on Burmese amber based on U-Pb dating of zircons. Cretac Res, 2012, 37: 155–163
90 Chen X, Yang S, Chen G, *et al*. Massive water production from lunar ilmenite through reaction with endogenous hydrogen. Innovation, 2024, 5: 100690
91 Donald IW, Metcalfe BL, Taylor RNJ. The immobilization of high level radioactive wastes using ceramics and glasses. J Mater Sci, 1997, 32: 5851–5887
92 Sacha GA, Saffell-Clemmer W, Abram K, *et al*. Practical fundamentals of glass, rubber, and plastic sterile packaging systems. Pharm Dev Tech, 2010, 15: 6–34
93 Lee YJ, Kim MS. Advances in drug-loaded microspheres for targeted, controlled, and sustained drug delivery: potential, applications, and future directions. Biomed Pharmacother, 2025, 189: 118244
94 Zachariasen WH. The atomic arrangement in glass. J Am Chem Soc, 1932, 54: 3841–3851
95 Kulcinski GL, Schmitt H. The moon: an abundant source of clean and safe fusion fuel for the 21st century. Lunar Helium-3 and Fusion Power, 1988, 1: 35–64
96 Simko T, Gray M. Lunar helium-3 fuel for nuclear fusion. World Futures Rev, 2014, 6: 158–171
97 Ouyang ZY, Li CL, Zou YL, *et al*. Primary scientific results of Chang'e-1 lunar mission. Sci China Earth Sci, 2010, 53: 1565–1581
98 Walsh CA, Yuan J, Brown LM. A procedure for measuring the helium density and pressure in nanometre-sized bubbles in irradiated materials using electron-energy-loss spectroscopy. Philos Mag A, 2000, 80: 1507–1543
99 David ML, Alix K, Pailloux F, *et al*. *In situ* controlled modification of the helium density in single helium-filled nanobubbles. J Appl Phys, 2014, 115: 123508
100 Ivanov AV. Volatiles in lunar regolith samples: a survey. Sol Syst Res, 2014, 48: 113–129
101 Trinkaus H, Singh BN. Helium accumulation in metals during irradiation—Where do we stand? J Nucl Mater, 2003, 323: 229–242
102 Trinkaus H. Energetics and formation kinetics of helium bubbles in metals. Radiat Effects, 1983, 78: 189–211
103 Jin S, Hao M, Guo Z, *et al*. Evidence of a hydrated mineral enriched in water and ammonium molecules in the Chang'e-5 lunar sample. Nat Astron, 2024, 8: 1127–1137
104 Lin H, Li S, Xu R, *et al*. *In situ* detection of water on the Moon by the Chang'e-5 lander. Sci Adv, 2022, 8: eabl9174
105 He H, Ji J, Zhang Y, *et al*. A solar wind-derived water reservoir on the Moon hosted by impact glass beads. Nat Geosci, 2023, 16: 294–300
106 Liu Y, Guan Y, Zhang Y, *et al*. Direct measurement of hydroxyl in the lunar regolith and the origin of lunar surface water. Nat Geosci, 2012, 5: 779–782
107 Zeng X, Tang H, Li XY, *et al*. Experimental investigation of OH/H_2O in H^+-irradiated plagioclase: implications for the thermal stability of water on the lunar surface. Earth Planet Sci Lett, 2021, 560: 116806
108 Kennedy D, Norman C. What don't we know? Science, 2005, 309: 75

Acknowledgement The authors thank the collaborators, Professors Weihua Wang, Haiyang Bai, Mengfei Yang, Zhigang Zou and others who work together in studying the physical properties of lunar regolith. We appreciate all the staff of Chang'e Lunar Exploration Project for their wonderful work in returning lunar samples and China National Space Administration for providing the lunar sample. This work was supported by the National Natural Science Foundation of China (52525105, U25A20216), Zhejiang Provincial Natural Science Foundation of China (LRG26E010001), and Youth Science and Technology Innovation Leading Talent Project of Ningbo (2024QL001).

Author contributions Wang J-Q, Gao M, Huo J and Huang Y designed and conceived the ideas for this review; Huang Y and Chen X summarized the literature; Huang Y wrote the initial manuscript; Huang Y, Gao M, Chen X and Wang J-Q revised the manuscript and put forward creative suggestions to improve the depth and coverage of the review; All authors contributed to the general discussion.

Conflict of interest The authors declare that they have no conflict of interest.

© Science China Press 2026

Yue Huang received her BE degree in materials forming and control engineering from Dalian University in 2022. She is currently a jointly cultivated master's student at Ningbo University and the Ningbo Institute of Materials Technology and Engineering, Chinese Academy of Sciences. Her master's research focuses on the mechanical and magnetic properties of molten lunar regolith.

Xiao Chen received his PhD degree from the Ningbo Institute of Materials Technology and Engineering, Chinese Academy of Sciences, in 2025. Now he works as a postdoctoral fellow at the Ningbo Institute of Materials Technology and Engineering, Chinese Academy of Sciences. His research interests include the physical properties of glassy materials in lunar soil and the *in situ* utilization of lunar resources.

Meng Gao received his PhD degree from the Institute of Physics, Chinese Academy of Sciences, in 2016. Then he worked as a postdoctoral fellow at the University of Wisconsin-Madison (USA) from 2016 to 2021. Now he is a professor at the Ningbo Institute of Materials Technology and Engineering, Chinese Academy of Sciences. His research interests include the characterization and regulation of heterogeneous structures in amorphous alloys.

Juntao Huo received his PhD degree from the Institute of Physics, Chinese Academy of Sciences, in 2012. Now he is a professor at Ningbo Institute of Materials Technology and Engineering, Chinese Academy of Sciences. His research focuses on magnetocaloric and electrochemical functional properties of amorphous alloys.

Jun-Qiang Wang received his PhD degree from the Institute of Physics, Chinese Academy of Sciences, in 2010. Then he worked as a postdoctoral fellow at Tohoku University (Japan) and the University of Wisconsin-Madison (USA) from 2010 to 2014. Now he is a distinguished professor at Ningbo Institute of Materials Technology and Engineering, Chinese Academy of Sciences. His research interests include non-equilibrium thermodynamics and functional properties of glassy materials.

月壤玻璃的性能和重要价值

黄越[1,2†], 陈霄[2†], 宋丽建[2], 许巍[2], 高萌[2*], 霍军涛[2,3*], 王军强[2,3*]

摘要 月球玻璃是月球上在陨石撞击、火山喷发等过程中形成的独特非晶材料, 既是记录月球演化的地质档案, 也是高真空、辐射和温度剧烈变化等极端环境下物质的天然储库. 本文系统综述了月球玻璃的科学认识、资源潜力和材料科学意义. 基于阿波罗和嫦娥五号采样数据, 梳理其分类与形成机制, 揭示了不同地质背景下的演化规律; 总结了多尺度结构特征及热稳定性、力学、辐照响应等关键物理性能; 评估了月壤玻璃中水和^{3}He的资源价值及其在月球原位资源利用中的作用; 最后, 从材料视角讨论月球玻璃在长期时间和离子辐照下的缺陷演化与纳米结晶过程, 并探讨了其对非晶合金和软磁材料设计的启示, 为极端环境下非晶物质的结构-性能调控提供参考.

© Science China Press 2026